Large-Scale Climate Modes Drive Low-Frequency Regional Arctic Sea Ice Variability

CHRISTOPHER WYBURN-POWELL[a] AND ALEXANDRA JAHN[a]

[a] *Department of Atmospheric and Oceanic Sciences, and Institute of Arctic and Alpine Research, University of Colorado Boulder, Boulder, Colorado*

(Manuscript received 2 June 2023, in final form 14 March 2024, accepted 6 May 2024)

ABSTRACT: Summer Arctic sea ice is declining rapidly but with superimposed variability on multiple time scales that introduces large uncertainties in projections of future sea ice loss. To better understand what drives at least part of this variability, we show how a simple linear model can link dominant modes of climate variability to low-frequency regional Arctic sea ice concentration (SIC) anomalies. Focusing on September, we find skillful projections from global climate models (GCMs) from phase 6 of the Coupled Model Intercomparison Project (CMIP6) at lead times of 4–20 years, with up to 60% of observed low-frequency variability explained at a 5-yr lead time. The dominant driver of low-frequency SIC variability is the interdecadal Pacific oscillation (IPO) which is positively correlated with SIC anomalies in all regions up to a lead time of 15 years but with large uncertainty between GCMs and internal variability realization. The Niño-3.4 index and Atlantic multidecadal oscillation have better agreement between GCMs of being positively and negatively related, respectively, with low-frequency SIC anomalies for at least 10-yr lead times. The large variations between GCMs and between members within large ensembles indicate the diverse simulation of teleconnections between the tropics and Arctic sea ice and the dependence on the initial climate state. Further, the influence of the Niño-3.4 index was found to be sensitive to the background climate. Our results suggest that, based on the 2022 phases of dominant climate variability modes, enhanced loss of sea ice area across the Arctic is likely during the next decade.

SIGNIFICANCE STATEMENT: The purpose of this study is to better understand the drivers of low-frequency variability of Arctic sea ice. Teasing out the complicated relationships within the climate system takes a large number of examples. Here, we use 42 of the latest generation of global climate models to construct a simple linear model based on dominant named climate features to predict regional low-frequency sea ice anomalies at a lead time of 2–20 years. In 2022, these modes of variability happen to be in the phases most conducive to low Arctic sea ice concentration anomalies. Given the context of the longer-term trend of sea ice loss due to global warming, our results suggest accelerated Arctic sea ice loss in the next decade.

KEYWORDS: Arctic; Sea ice; Climate variability; Climate models

1. Introduction

Over the past four decades, summer Arctic sea ice has rapidly declined and is projected to continue to decline in the future (Wang and Overland 2012; Notz and Stroeve 2016; Sigmond et al. 2018). However, large variability on multiple time scales is superimposed on this declining trend, which can lead not only to 10–20-yr periods of accelerated sea ice loss but also to a period of over a decade of no sea ice loss (Kay et al. 2011; Swart et al. 2015). Hence, it is not unexpected that no new record low September sea ice area has occurred since 2012 (Francis and Wu 2020), in particular as September internal variability is currently elevated due to the decrease in the thickness and mean sea ice state (Goosse et al. 2009; Eisenman 2010; Jahn 2018; Mioduszewski et al. 2019). The shelf seas have been the focus of the observed decline as well as of the impact of internal variability, with lower average sea ice concentration and thinner ice making the area a hotspot of internal variability over the past few decades (Lindsay and Zhang 2006; England et al. 2019; VanAchter et al. 2020; Årthun et al. 2021). The shelf seas are also coincident with areas of interest for shipping (Eguíluz et al. 2016; Melia et al. 2017), natural resource exploration (Petrick et al. 2017), and ecological changes (Kovacs et al. 2011). However, the current characteristics of variability are likely transitory as the shelf seas in the next few decades will become more reliably ice-free throughout the summer (Barnhart et al. 2016; Crawford et al. 2021), ending the dominant role of internal variability in projection uncertainty for this region (Bonan et al. 2021).

The internal variability of Arctic sea ice acts on multiple time scales and has therefore been challenging to cleanly separate from the forced response (Stroeve et al. 2007; Kay et al. 2011; Swart et al. 2015; Dörr et al. 2023). High-frequency drivers such as atmospheric temperature and wind anomalies are generally considered dominant over lower-frequency drivers (Ding et al. 2019; Olonscheck et al. 2019; Roach and Blanchard-Wrigglesworth 2022), but separating the drivers is difficult due to large spatial and temporal heterogeneity in

Supplemental information related to this paper is available at the Journals Online website: https://doi.org/10.1175/JCLI-D-23-0326.s1.

Corresponding author: C. Wyburn-Powell, chwy8767@colorado.edu

DOI: 10.1175/JCLI-D-23-0326.1

variability (Onarheim et al. 2018). By defining low-frequency variability as periods of at least 2 years, approximately one-quarter of September pan-Arctic internal variability can be accounted for by low-frequency variability in a sample of global climate models (GCMs) (Wyburn-Powell et al. 2022). Although low-frequency variability is only a small component of internal variability, it promises some longer-term predictability, as the influence of initial conditions and high-frequency drivers of variability decay rapidly beyond the current season (Blanchard-Wrigglesworth et al. 2011; Bonan et al. 2019; Bushuk et al. 2019) and have been shown to be useful to a maximum of 2-yr lead time (Day et al. 2014; Yeager et al. 2015; Bushuk and Giannakis 2017; Holland et al. 2019; Gregory et al. 2022; Wang et al. 2021).

There is some prospect of summer Arctic sea ice predictability at lead times greater than 2 years due to ocean heat transports (Zhang 2015; Docquier et al. 2021) and climate modes of variability (Guemas et al. 2016). However, results so far seem to be model dependent (Tietsche et al. 2014; Blanchard-Wrigglesworth and Bushuk 2019), and our current length of observations is likely too short to verify such relationships (Bonan and Blanchard-Wrigglesworth 2020; Karami et al. 2023). Despite these challenges, extratropical modes of sea level pressure variability have been suggested to directly affect Arctic sea ice variability but so far only with strong evidence on high-frequency time scales (Ukita et al. 2007; Serreze et al. 2007; L'Heureux et al. 2008; Zhang et al. 2019; Liu et al. 2021). Tropical teleconnections have also been identified as influencing Arctic sea ice loss, primarily associated with Pacific sea surface temperatures (SSTs) (Hu et al. 2016; Li et al. 2018a; Screen and Deser 2019; Ding et al. 2019; Kim et al. 2020; Clancy et al. 2021; Jeong et al. 2022b; Simon et al. 2022) but also with Atlantic variability (Day et al. 2012; Miles et al. 2014; Meehl et al. 2018; Li et al. 2018b; Karami et al. 2023). Rossby wave trains are the primary mechanism linking tropical Pacific SST anomalies to the Arctic (Yuan et al. 2018). These Rossby waves propagate from the tropics to the Arctic on the order of 2 weeks (Alexander et al. 2002) but can have seasonal Arctic sea ice effects due to persistent positive geopotential height anomalies and associated subsidence and diabatic warming leading to reduced sea ice cover (Baxter et al. 2019; Hofsteenge et al. 2022). These insights into drivers of variability show promise, but skillful regional sea ice predictions combining multiple modes of variability at lower-frequency time scales have so far been elusive.

Assessing drivers of low-frequency variability in the climate system is difficult to do without large quantities of consistent data, such as that available from single-model initial-condition large ensembles (Deser et al. 2020; Milinski et al. 2020). This requirement for assessing drivers of low-frequency Arctic sea ice variability stems from a multitude of drivers likely interacting on heterogeneous spatial and temporal scales to cause this variability (Zhang et al. 2020). This has, so far, led to a lack of consensus among many of the drivers at time periods in excess of 2 years, especially as GCMs and observations have been shown to represent these relationships differently. We therefore leverage all available GCMs from phase 6 of the Coupled Model Intercomparison Project (CMIP6) archive to investigate the model consensus of these low-frequency relationships. Additionally, we do not prescribe the nature of any of these relationships such as linearity and independence, and we perform a detailed regional analysis as well as assess multiple lead times. To enable interpretation of these potentially complex relationships in the climate system, we use machine learning which has been used successfully before to explain patterns of surface climate variability (e.g., Barnes et al. 2019; Labe and Barnes 2022). With this coherent approach to determine the drivers of low-frequency Arctic sea ice variability on multiple time scales and locations, we determine the modes of variability which are simulated to have the largest impact and use the resulting model to make predictions of low-frequency sea ice concentration (SIC) variability over the next decade.

2. Methods

a. *Data sources*

To gather sufficient data on both climate modes of variability and associated sea ice concentrations, we use 42 GCMs with historical CMIP6 forcing (O'Neill et al. 2016). These GCMs are those for which monthly sea ice concentration is available and the full suite of climate mode data has been processed using the Climate Variability Diagnostics Package (CVDP) (Phillips et al. 2014). In total, we use 609 realizations, from 42 GCMs and 23 modeling centers; a full list can be found in Table 1. In using the full suite of CMIP6 GCMs, we can get a consensus of low-frequency drivers of Arctic sea ice variability, as individual GCMs have biases in their simulation of teleconnections (Dalelane et al. 2023), but some systematic biases pervasive across CMIP5 are improved in CMIP6 (Fasullo et al. 2020).

Alternatives to the historical simulations which could provide a similarly large quantity of data include future scenarios or preindustrial control simulations. However, as the mean state and variability of the Arctic sea ice (VanAchter et al. 2020; Årthun et al. 2021) and some aspects of the rest of the climate system such as El Niño–Southern Oscillation (ENSO) (Brown et al. 2020) or Atlantic meridional overturning circulation (AMOC) (Weijer et al. 2020) differ from present conditions, this approach would be less appropriate to analyze near-contemporaneous variability. Despite differences in the mean state, we do utilize preindustrial control simulations to assess the validity of our detrending methodologies, but not make projections, as detailed in section 2d.

Within the historical period, we use the 95-yr time period 1920–2014 for SIC, which we average over regions of the Arctic as defined by the National Snow and Ice Data Center (NSIDC) multisensor analyzed sea ice extent—Northern Hemisphere (MASIE-NH) (Fetterer et al. 2010) (see Fig. 1d). These seven regions cover the vast majority of the sea ice found during the summer although we do exclude the Canadian Arctic Archipelago due to complex coastal zones which are typically poorly represented in GCMs (Long et al. 2021). We linearly detrend the average SIC for each region and then

TABLE 1. GCM output used in this analysis.

Modeling center	GCM name	Members	Citation
CSIRO-ARCCSS	ACCESS-CM2	5	Dix et al. (2019)
CSIRO	ACCESS-ESM1.5	40	Ziehn et al. (2019)
BCC	BCC-CSM2-MR	3	Wu et al. (2018)
BCC	BCC-ESM1	3	Zhang et al. (2018)
CAMS	CAMS-CSM1.0	3	Rong (2019)
NCAR	CESM2-FV2	3	Danabasoglu (2019a)
NCAR	CESM2-LENS	50	Danabasoglu (2019b)
NCAR	CESM2-WACCM	3	Danabasoglu (2019d)
NCAR	CESM2-WACCM-FV2	3	Danabasoglu (2019c)
THU	CIESM	3	Huang (2019)
CMCC	CMCC-CM2-SR5	11	Lovato and Peano (2020)
CNRM-CERFACS	CNRM-CM6-1	21	Voldoire (2018)
CNRM-CERFACS	CNRM-ESM2-1	6	Seferian (2018)
CCCma	CanESM5	65	Swart et al. (2019b)
CCCma	CanESM5-CanOE	3	Swart et al. (2019a)
E3SM-Project	E3SM1.0	4	Bader et al. (2019)
EC-Earth Consortium	EC-Earth3	23	EC-Earth-Consortium (2019a)
EC-Earth Consortium	EC-Earth3-CC	10	EC-Earth-Consortium (2021)
EC-Earth Consortium	EC-Earth3-Veg	7	EC-Earth-Consortium (2019b)
EC-Earth Consortium	EC-Earth3-Veg-LR	3	EC-Earth-Consortium (2020)
FIO-QLNM	FIO-ESM2.0	3	Song et al. (2019)
NOAA–GFDL	GFDL-ESM4	3	Krasting et al. (2018)
NASA-GISS	GISS-E2.1-G	46	NASA Goddard Institute for Space Studies (2018)
NASA-GISS	GISS-E2.1-H	25	NASA Goddard Institute for Space Studies (2019b)
NASA-GISS	GISS-E2.2-G	11	NASA Goddard Institute for Space Studies (2019a)
NASA-GISS	GISS-E2.2-H	5	NASA Goddard Institute for Space Studies (2019c)
MOHC	HadGEM3-GC31-LL	5	Ridley et al. (2019a)
MOHC	HadGEM3-GC31-MM	4	Ridley et al. (2019b)
INM	INM-CM5-0	10	Volodin et al. (2019)
IPSL	IPSL-CM6A-LR	32	Boucher et al. (2018)
MIROC	MIROC-ES2H	3	Watanabe et al. (2021)
MIROC	MIROC-ES2L	31	Hajima et al. (2019)
MIROC	MIROC6	50	Tatebe and Watanabe (2018)
HAMMOZ-Consortium	MPI-ESM1.2-HAM	3	Neubauer et al. (2019)
MPI-M	MPI-ESM1.2-HR	10	Schupfner et al. (2019)
MPI-M	MPI-ESM1.2-LR	30	Wieners et al. (2019)
MRI	MRI-ESM2	12	Yukimoto et al. (2019)
NUIST	NESM3	5	Cao and Wang (2019)
NCC	NorCPM1	30	Bethke et al. (2019)
NCC	NorESM2-LM	3	Seland et al. (2019)
NCC	NorESM2-MM	3	Bentsen et al. (2019)
MOHC	UKESM1.0-LL	16	Tang et al. (2019)

apply a 2-yr low-pass filter to exclude the high-frequency interannual variability and leave only the low-frequency anomalies (see Figs. 1a–c). These low-pass-filtered regional sea ice concentration data become the predictands in our regression analysis.

We use nine variables from the CVDP to assess their influence on regional SIC anomalies in our regression analysis. We have included a brief description of these modes of variability below; we have also included a citation of a relevant article using the same index. These climate modes of variability aim to capture different aspects of variability within the climate system although some of these do overlap in spatial or temporal domains and thus should not be considered independent. We obtain seasonal values for all variability modes which are then linearly detrended over the period 1920–2014 and standardized (if not already in such a format). As we lag the SIC data between 2 and 20 years from the CVDP data, only the latest 74 years of the 95-year time period are used for a given lag time (1941–2014). When we present the linear effects of each mode of variability, we only use one seasonal value for the climate modes listed below (see section 2b for selection of the season):

- Atlantic multidecadal oscillation (AMO; winter—DJF): The area-weighted SST anomalies in the North Atlantic basin (0°–60°N, 0°–80°W), which is thought to have a period of approximately 60–80 years (Trenberth and Shea 2006).
- North Atlantic Oscillation (NAO; winter—DJF): The leading principal component of the Atlantic (20°–80°N, 90°W–40°E) seasonal average sea level pressure anomalies. The positive

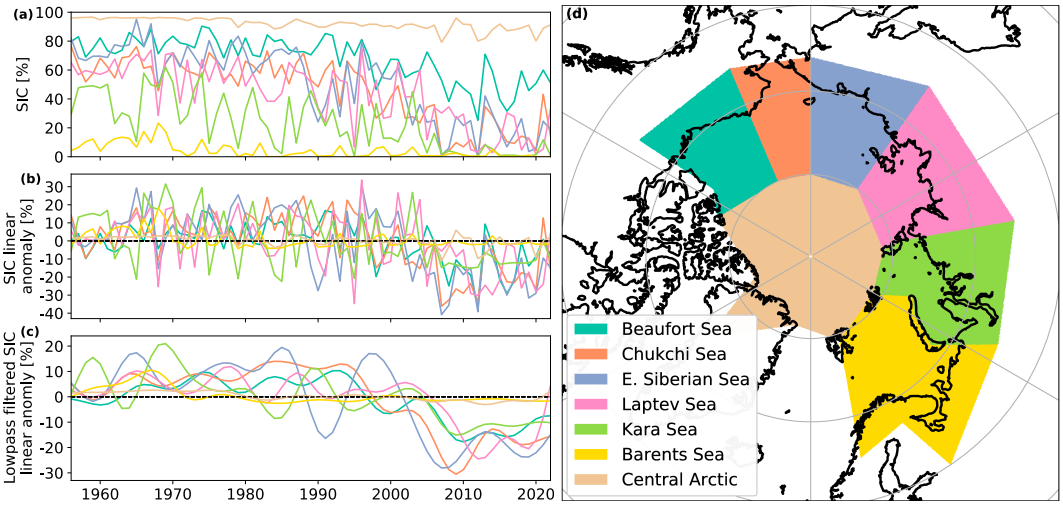

FIG. 1. Observed September SICs for the seven Arctic regions used in this analysis. The observational HadISST1 SIC data are shown for (a) the regional average, (b) the linearly detrended version of (a), and (c) a 2-yr low-pass filter applied on (b). The data used in the analysis presented here are shown in (c). (d) The outline of the different regions considered is shown and defined as for the NSIDC MASIE-NH dataset (Fetterer et al. 2010).

phase indicates a relatively enhanced Azores high and a deepened Icelandic low (Hurrell and Deser 2009). The NAO may have some small decadal predictability, such as from the AMO, but is dominated by large interannual variability (Klavans et al. 2021).

- Atlantic Niño (ATN; spring—MAM): The area-averaged tropical Atlantic SST anomalies (3°S–3°N, 0°–20°W), with a similar periodicity to the Pacific El Niño/La Niña phases (Zebiak 1993).
- Niño-3.4 index (NINO34; winter—DJF): Five-month running mean SST anomalies in the equatorial Pacific (5°N–5°S, 120°–170°W). Values continuously in excess of +0.4°C for 6 months indicate El Niño conditions; values continuously below −0.4°C indicate La Niña (Trenberth 1997). Such oscillations between positive and negative states occur approximately every 2–7 years in the observational record.
- Pacific decadal oscillation (PDO; spring—MAM): The leading principal component of north Pacific SST anomalies (20°–70°N, 110°E–100°W). Positive phases are associated with positive SST anomalies in the eastern Pacific and negative SST anomalies in the western and central Pacific (Mantua et al. 1997). The PDO is thought to have a periodicity of approximately 50–70 years over the last 200 years (MacDonald and Case 2005).
- North Pacific Oscillation (NPO; spring—MAM): The second principal component of seasonal sea level pressures over the North Pacific and North American continent (20°–85°N, 120°E–120°W) (Phillips et al. 2014). A positive phase is indicative of a deepened Aleutian low and enhanced sea level pressure in the region of 20°–40°N as per Rogers (1981) who defined the NPO based on geopotential height. A given phase usually persists on the order of a week.
- Pacific–North American teleconnection (PNA; spring—MAM): The leading principal component of seasonal sea level pressures over the North Pacific and North American continent (20°–85°N, 120°E–120°W) (Phillips et al. 2014). A positive phase is similar to the NPO with a deepened Aleutian low, but this mode of variability is more extensive, also including enhanced pressure over western Canada [see Leathers et al. (1991) who used geopotential height anomalies].
- Interdecadal Pacific oscillation (IPO; spring—MAM): The leading principal component of 13-yr low-pass-filtered Pacific (40°S–60°N, 110°E–70°W) area-weighted SST anomalies. In its positive phase, SST anomalies in the equatorial Pacific are positive with the western extratropical Pacific in both hemispheres experiencing cooler SST anomalies (Meehl et al. 2013). The period and symmetry of the IPO are thought to have varied considerably over time, but over the observational period, it has been shown to change phase approximately every 20–30 years (Vance et al. 2022).

In addition to these modes of variability, we also include the summer (JJA) global average surface temperature (TAS), as motivated in section 2d.

Several additional modes of variability were also available from the CVDP but were not included in the final analysis. The modes investigated but not used are as follows: the Indian Ocean dipole, the Atlantic meridional mode, the Southern Annular Mode, and the North Pacific index. All of these modes of variability had no measurable effect on the regression model. Furthermore, including the Northern Annular Mode led to overfitting with the highly related NAO.

To compare model results to observations, we use SIC from the Hadley Centre Sea Ice and Sea Surface Temperature dataset (HadISST1) (Rayner et al. 2003) for the period 1956–2022. We use the HadISST1 SIC record before the beginning of the satellite era in 1978 to enable longer analyses in our correlation analysis in section 3e. We started using the HadISST1 SIC data in 1956, as the variability was degraded

substantially before 1956 due to interpolations during winter (Rayner et al. 2003). However, when calculating linear trends for detrending, we use SIC data for 1920–2014 in order to be consistent with the GCMs. This is possible due to moderate confidence in the mean state for 1920–55 despite the increased uncertainty in the interannual sea ice variability for that period. The HadISST1 data, similarly to the SIC in the GCMs, are divided into regions; linearly detrended and interannual variability is removed with a 2-yr low-pass filter. For observed climate variability data, we also obtain these from the CVDP where we use the HadISST1 dataset to calculate sea surface temperature–derived variables, the NCEP–NCAR record for sea level pressures (Kalnay et al. 1996), and GISTEMP, version 4, for global surface temperatures (Lenssen et al. 2019). Similarly to the CVDP output variables for the GCMs, we apply linear detrending and standardization to the variables not already in this format.

b. *Machine learning methods*

To determine the relationship between the climate variability modes and the lagged effects on regional Arctic SIC gain and loss, we use machine learning. Specifically, we use neural networks which excel at finding relationships within large datasets (e.g., Diffenbaugh and Barnes 2023). At its simplest, the neural networks used here are multiple linear regression, but we can also account for nonlinear relationships and covariance by using more advanced neural network configurations. To constrain the potentially complicated relationships between climate modes and subsequent SIC changes, we require large quantities of data to train, validate, and test our neural networks. We therefore utilize three datasets as listed below, which fulfill different purposes:

- Twelve large ensembles (LEs): individual CMIP6 GCM large ensembles of at least 20 members.
- Multimodel large ensemble (MMLE) 3+: all CMIP6 GCMs (42) with at least three members.
- MMLE 30+: all CMIP6 GCMs (8) with at least 30 members.

To determine the climate mode relationships with Arctic sea ice within an individual GCM, we require at least 20 members to provide sufficient data. This means we can train a neural network separately on 12 of the 42 GCMs, referred to as LEs. To get a consensus across the 42 CMIP6 GCMs and weigh them equally, we train a neural network on the first members of all 42 GCMs, validate on the second members, and test on the third members (the MMLE 3+). Finally, we also train a neural network on the first 23 members of 8 GCMs with sufficiently large ensembles; this allows us to see whether maximizing the available data increases predictive skill (MMLE 30+).

For all LEs, MMLE 3+, and MMLE 30+, we use a single seasonal time series from eight climate modes and TAS to predict lagged sea ice anomalies at one lead time, one region, and one sea ice anomaly month at a time. This allows any patterns between the lags, regions, or sea ice anomaly months to be discovered rather than prescribed. The SIC anomalies are in percentage points for consistency across regions. Hence, when comparing the influence of modes of variability in the aggregate, the percentage point change should be scaled by the variability of that region (as is done for Fig. 8). The use of percent SIC deviation from the trend has identical meaning to using sea ice area and is not sensitive to the mean state, other than the 0%–100% bounds capping anomalies. The neural networks have no knowledge of the initial sea ice state, but as the memory for the summer at lead times in excess of 1 year is considered negligible (Giesse et al. 2021), this omission is considered unimportant at the time scales we consider. Further, including initial sea ice state as a predictand would add complexity to our methods which would be difficult to constrain without additional data.

We utilize four configurations of machine learning model to test whether nonlinearities and covariance between the climate modes are required to make skillful predictions of Arctic sea ice anomalies. We achieve this by constructing four models listed below differing in their linear or nonlinear relationships (activation functions) and whether they take into account climate mode covariance (presence or absence of hidden layers). Model 1 has independent linear relationships between the climate modes and sea ice anomalies and hence is effectively multiple linear regression. Model 2 is the same as model 1 but permits nonlinear relationships. Model 3 uses only linear relationships but can take advantage of covariance between climate modes, such as a positive phase of the IPO and a positive phase of the PDO having a different combined effect than the individual effect of those modes. Model 4 is the most complicated, allowing both nonlinear relationships and also covariance between the modes of variability. For further details on the machine learning models, see section S1 in the online supplemental material.

c. *Assessing predictive skill*

The threshold for our machine learning model to be useful at a given lag time is defined as when its Pearson correlation coefficient for the validation data exceeds that obtained from persistence. The persistence correlation coefficient in this instance is calculated from the 2-yr low-pass-filtered regional SIC anomalies lagged between 2 and 20 years, the same lag times as used for our regression analysis. When using the correlation coefficient, it is important to note that, especially at longer lag times, there may be a high correlation between the linear model output and the validation data, but this skill may be present with a smaller amplitude than for the validation data. Further, for regions that are close to zero or 100% SIC, we are trying to predict very small variations in SIC. Hence, we could have poor predictability in these regions but still have small errors in absolute terms.

As we do not have sufficiently long periods of observations, we cannot train a separate machine learning model on the observations. Instead, by pooling several regions and SIC anomaly months, we calculate the proportion of positively and negatively correlated modes of variability with the most extreme 10% of SIC positive and negative anomalies. This is not a way of verifying the GCM predictive models per se; rather, it shows the range of correlations present within a large ensemble and allows observation to be placed alongside

that range. Observations would be expected to typically fall within the large ensemble distribution, but as we do not know how atypical our one realization of reality is, we cannot ascribe meaning to differences from the ensemble mean (Notz 2015). Similarly, when in section 3e we provide predictions of past and future regional SIC anomalies, good agreement to observations does not explicitly validate our results.

d. Sensitivities to time period and forcing

We use a linear detrending for both the SIC and the CVDP variables over the period 1920–2014 as this is a simple process to understand and does not make specific assumptions about the time period in question. This is not perfect as, during that period, the radiative forcing as well as the observed and modeled sea ice decline were not entirely linear (see Fig. 1 of McBride et al. 2021 for global temperature). This means that some of the very low-frequency variability of the forced response is incorporated into the anomalies of SIC and CVDP variables, rather than being removed by detrending. Therefore, some predictability is due to the shape of the forced response, primarily represented by our input variable of global average surface temperature (TAS), and likely, to a small extent, the SST-derived variables of NINO34, PDO, ATN, AMO, and IPO. As the simple linear model used in our results considers each variable independently, we can consider TAS similarly to a residual term in the model which does not affect the conclusions we draw about other modes of variability.

To verify that our results from the period 1920–2014 are robust to different forcing conditions, we compare results with a more linear forcing scenario for the historical period 1970–2014 and a constant preindustrial forcing scenario. For the 1970–2014 time period, the global surface temperature and sea ice area trends are both highly linear (Notz and Stroeve 2016; McBride et al. 2021). Consequently, for 1970–2014, we find that the linear response to TAS in our models is far smaller than in 1920–2014 (see Fig. S1 compared with Fig. 4). The 1970–2014 time period, after accounting for lags, only uses 24 years of data (compared with 74 for 1920–2014), and hence, the linear response is much more noisy than for 1920–2014. Therefore, although we get broadly similar linear responses for each climate mode, the low skill relative to persistence means we cannot use this shorter time period despite the more linear variables and more similar mean states to the present day.

Preindustrial control runs (of which 35 GCMs are available to each provide 222 training years) use constant 1850 radiative forcing, and hence, TAS trends are near zero over a 74-yr time period. Despite the different mean state and variability, we still find very similar linear coefficients to the 1920–2014 time period but with a smaller influence of TAS (see Fig. S2 compared with Fig. 4). However, the preindustrial control results provide much smaller linear responses, likely due to the 1850 mean state exhibiting less variability than the twenty-first century, primarily due to thicker Arctic sea ice (Kwok and Rothrock 2009). Despite the preindustrial control climate being too different from the present day to make projections, the similar results to the 1920–2014 period imply that the relationships are inherent to the climate system, not artifacts of the detrending methodology, with the possible exception of NINO34 as discussed in section 4. We therefore use the 1920–2014 time period, despite the TAS and SIC nonlinearity, as it both captures similar SIC mean state and variability to the present day and enables the use of sufficient training data.

3. Results

a. A simple linear model captures drivers of low-frequency variability

Predictions of regional low-frequency Arctic sea ice concentration anomalies can be produced from climate modes of variability using a linear model, which are skillful when compared with persistence. In general, we find that the simple linear variant of the machine learning models (model 1) produces the highest predictive skill of the four models across GCMs, regions, and seasons. When validating our linear model, we find it generally exceeds the skill from persistence for lead times beyond approximately 4 years but is dependent on the GCM (see Fig. 2 for the Chukchi Sea in September). The highest predictive skill is found at approximately a 5-yr lead time when the r^2 value of persistence has decayed close to zero, while the r^2 value of the linear model declines more slowly with lead time. This temporal pattern of persistence, as well as the superiority of the linear model, is found across regions and months with nonzero skill (see section 3b).

The simple linear model with no hidden layers (model 1) and the linear neural network allowing climate mode covariance (model 3) are nearly identical in their performance across different LEs and MMLEs (see Fig. 2). The high performance of models 1 and 3 implies that nonlinearities are not required to produce a skillful predictive model. The simple nonlinear model 2 consistently performs poorly, with model 4 performing erratically for small training data, but can exceed the skill of other models for short lead times and for the largest LEs and MMLEs. As model 4 includes the effect of covariance of climate modes and nonlinearities, this complex relationship between climate modes and sea ice anomalies is shown to only provide a modest benefit to predictions. Subsequently, we therefore only utilize model 1, the simple linear model, to clearly determine the independent linear effect of each climate mode of variability. However, with additional data, the likely interdependent and nonlinear relationships may be able to be detected robustly to allow greater generalization and produce better predictions.

b. Hotspots of low-frequency variability predictive skill

The summer and autumn marginal seas are generally able to produce the highest skill at a 5-yr lead time; however, the predictive skill varies considerably between GCM. Based on the MMLE 3+, which takes into account the full suite of CMIP6 GCMs with at least three ensemble members, the pattern of highest predictability is found in the Beaufort Sea in September, with decaying skill for regions further from the Pacific and for months more distant from September (Fig. 3). The MMLE 3+ model is unable to produce high predictive

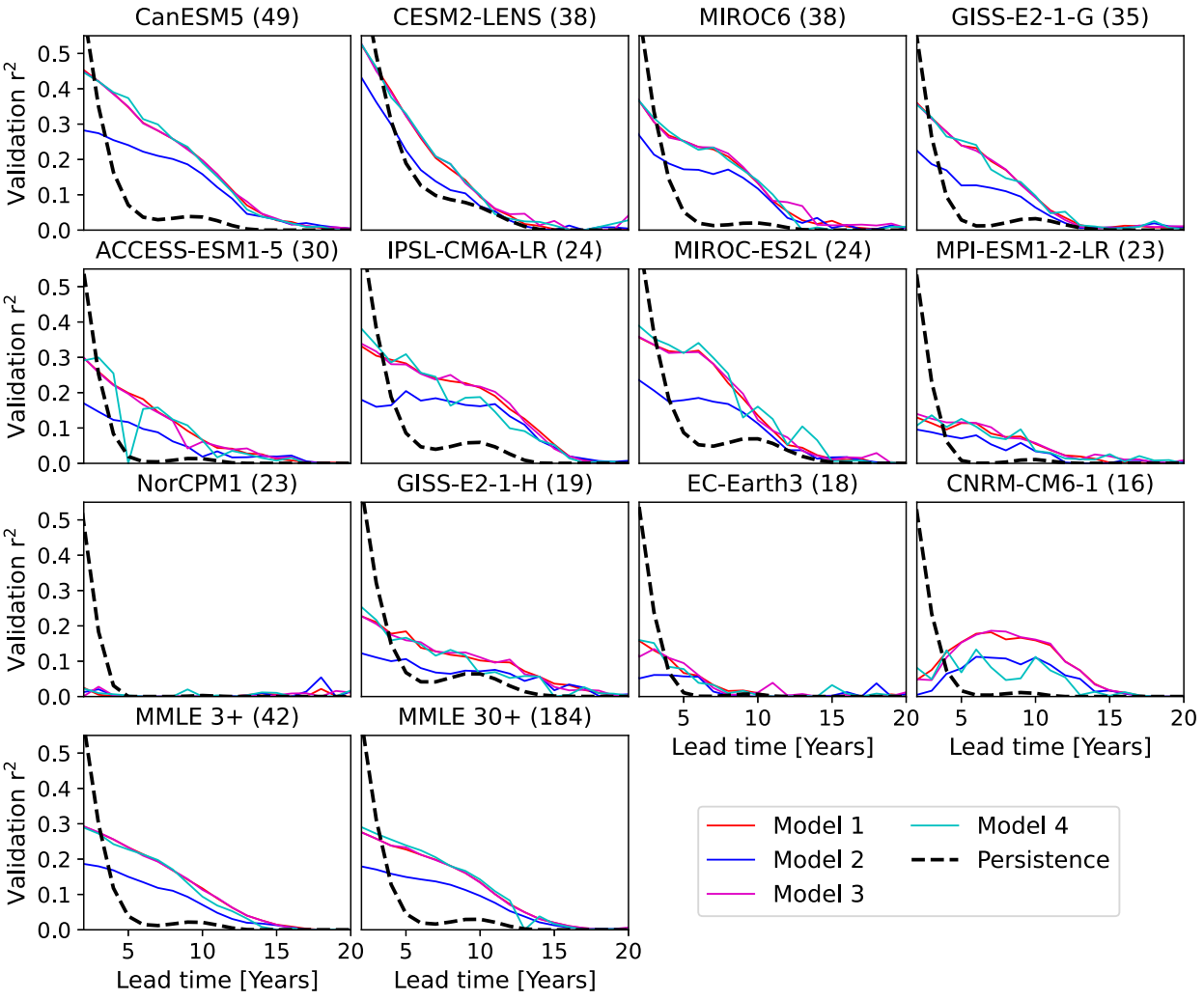

FIG. 2. The effect of machine learning model complexity on predictive skill. Pearson correlation coefficients in the Chukchi Sea in September for the validation data for four machine learning models are shown for the 12 LEs and 2 MMLE datasets. Model 1 refers to the simple linear model (red), model 2 refers to the simple nonlinear model (blue), and models 3 and 4 refer to the fully connected 9-3-3-1 neural network with linear (purple) and nonlinear (cyan) activation functions, respectively. The black dashed line indicates the average persistence for that lag time for the GCM or GCMs used. Where the model validation r^2 values exceed persistence, the model has predictive skill. The numbers in parentheses indicate the number of ensemble members used in training.

skill in the Barents Sea for any season likely due to frequently near-zero SIC, and the Kara Sea appears to have distinct peaks of predictive skill in July and late autumn.

For models using individual GCMs, the temporal and regional patterns of predictive skill are often noisy for neighboring regions and months, unlike the clearer MMLE models. The relatively high predictive skill values of the LEs typically exceed that of the MMLE 3+ for the best regions but with less coherence between regions and months. Selecting the LE with the highest skill for a region and month may be appropriate, but each LE's specific spatial and temporal limitations should be taken into account. The MMLE 3+ has lower predictive skill than the best LEs but is influenced by all 42 CMIP6 GCMs. Therefore, the relatively higher predictive skill in the MMLE 3+ should be seen as less sensitive to individual GCM biases as it is representative of the general agreement between all GCMs. Some LEs such as CanESM5 and ACCESS-ESM1-5 exhibit unusual patterns of high predictability in the Kara and Chukchi Seas in the winter. Other LEs such as CESM2-LENS, GISS-E2.1-H, and MIROC-ES2L have particular regions which are far more predictable than others. For example, the CESM2-LENS simulates high persistence for the Chukchi Sea but not for the Beaufort Sea (see Fig. S4 for 5-yr persistence and section 3f for a CESM2 bias discussion) which causes the large disparity in predictive skill between these two regions. As September is of particular interest as the typical minimum annual pan-Arctic sea ice cover and relatively high validation r^2 values occur across regions for September in the MMLE 3+, this is our focus in subsequent analyses.

c. *Linear drivers of regional sea ice anomalies*

Using a linear model trained on 42 CMIP6 GCMs (the MMLE 3+ model), we can establish the consensus across

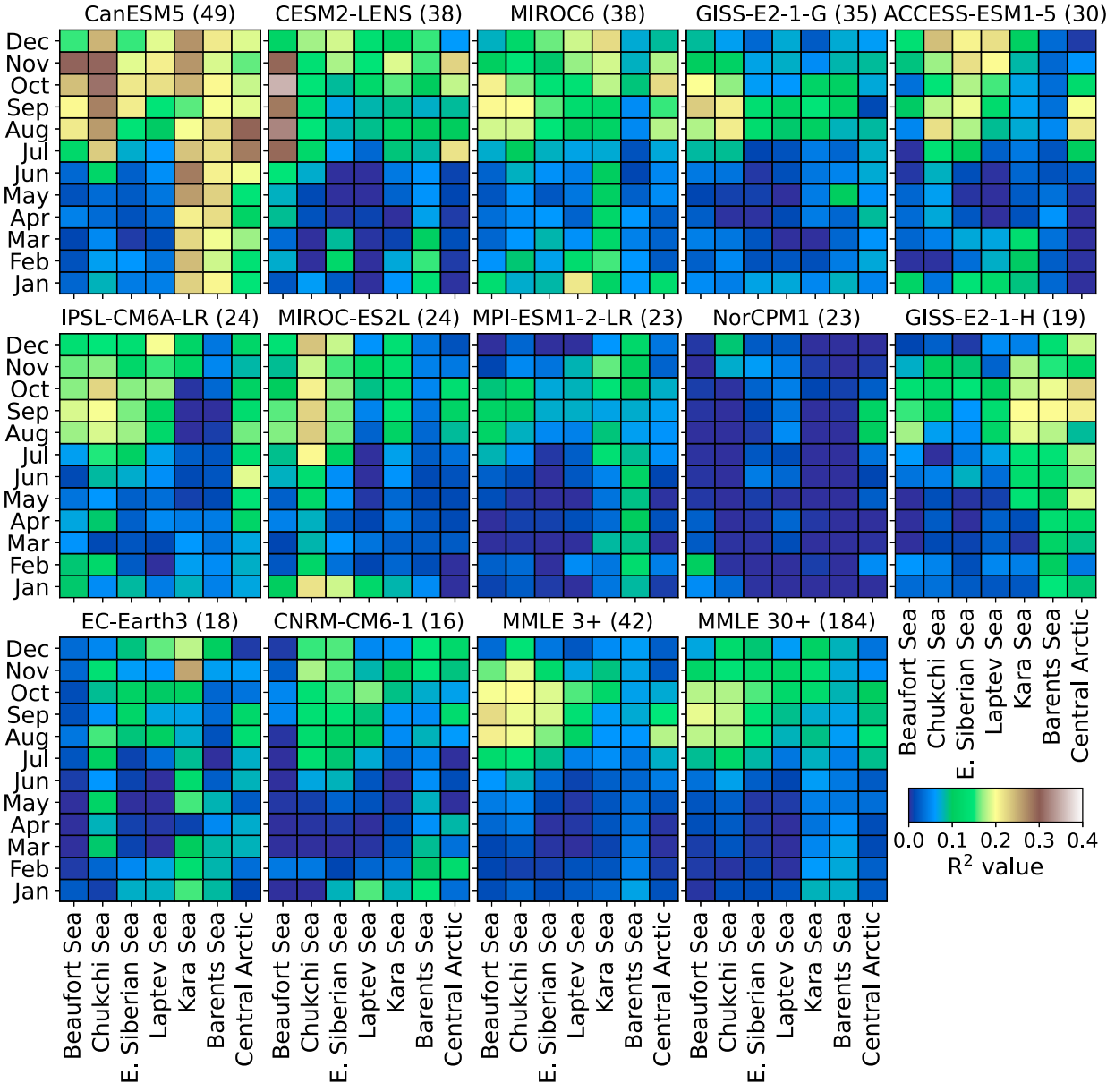

FIG. 3. Five-year lagged predictive skill for multiple GCMs and the CMIP6 multimodel ensembles. Pearson correlation coefficients are shown for the validation data minus persistence at a 5-yr lag time between the input climate modes and SIC anomalies. Persistence is removed to indicate the regions and months for each LE or MMLE where predictive skill is high, rather than where explained variability is high. Numbers in parentheses indicate the total number of ensemble members used for training.

GCMs for the independent effect of each mode of variability on regional September SIC anomalies. The lead times where the MMLE 3+ model has no predictive skill are before a 4-yr lead time for all regions except the central Arctic where it is not until a 5-yr lag time that the validation r^2 exceeds persistence (see the dotted lines in Fig. 4). The most important mode of variability is the IPO, which is strongly positively correlated with the SIC in all regions, especially in the East Siberian and Beaufort Seas (Fig. 4). The IPO decays in influence over time, reaching near-zero influence on SIC at approximately a 15-yr lead time. The global average surface temperature (TAS) also has very large coefficients, but as this is not a mode of variability and is considered to integrate modes of variability not represented (see section 2d for a more detailed explanation), we do not discuss in detail the influence of TAS further.

Aside from the large influence of the IPO, the NINO34 and the AMO both display a very consistent sign of influence which decays with time. The NINO34 and AMO both have smaller influences than the dominant IPO (approximately one-third and one-quarter, respectively) for a given one standard deviation anomaly in each mode of variability. Like the

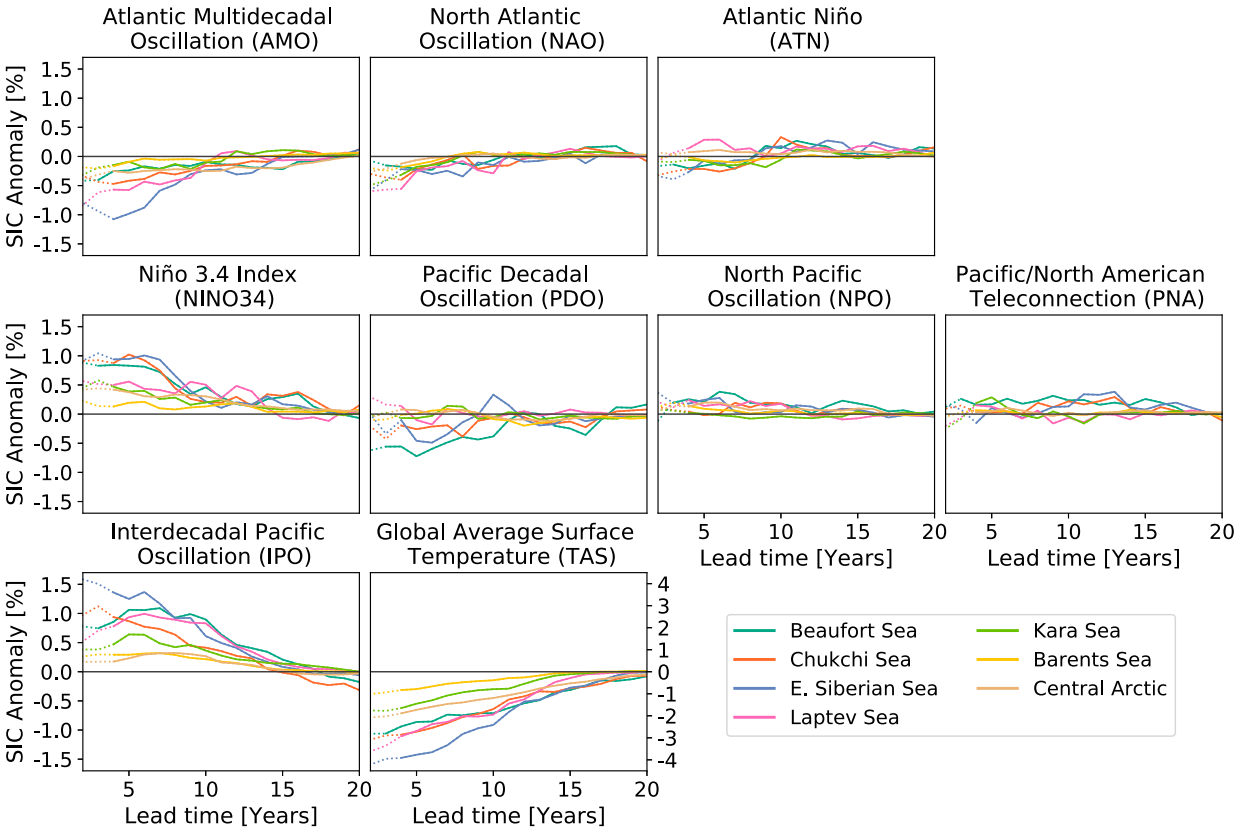

FIG. 4. Linear drivers of September regional SIC anomalies. Linear response of a +1 standard deviation anomaly of each of the eight climate modes and global average surface temperature on SIC anomalies in each of the seven Arctic regions. Positive SIC anomaly values indicate a positive SIC anomaly results from the +1 standard deviation anomaly in the climate mode of variability. Solid lines indicate that the validation r^2 value exceeds persistence for a given region and lead time, and dashed lines indicate where there is no predictive skill beyond persistence. Nonzero predictive skill occurs for 4–20-yr lead times for all regions except for the Beaufort Sea which has some predictive skill for a wider range of 3–20-yr lead times.

IPO and TAS, the influence of the AMO and NINO34 decays relatively monotonically with time. As the skill of persistence also declines nearly monotonically and the IPO, TAS, NINO34, and AMO all display low-frequency variability, this increases confidence in the validity of these relationships found in the MMLE 3+. The low-frequency oscillations of the other sea surface temperature–derived indices of the PDO, and to a lesser extent the ATN, imply the potential for longer-term predictability as with the IPO, TAS, NINO34, and AMO. However, the influence of these modes is small at most time periods and does not display a monotonic decline with time. This suggests these two modes are not highly important in driving low-frequency Arctic sea ice variability, but consistency or lack thereof between LEs (see section 3d) may clarify whether the relationships in the MMLE 3+ are small and independently consistent in magnitude between GCMs or small due to disagreement between GCMs.

The modes of variability based on sea level pressure patterns are generally a small influence on the low-frequency variability of Arctic sea ice. The PNA and NPO do have some coherent regional effects, but the switch in the sign of influence over time may be indicative of the expectation of a change in the mode itself rather than the effect of the initial sign of the mode. Further, the NPO and PNA are influenced by longer-lived modes of variability in the Pacific (Furtado et al. 2012), potentially meaning these modes are not independent. The NAO is less erratic than the NPO and PNA with a general negative effect on SIC anomalies but is very small in magnitude and is shown to affect SIC anomalies minimally.

d. *Low-frequency driver representation across global climate models*

Comparing the independent results from 12 LEs aids our interpretation of the linear drivers of SIC anomalies captured in the MMLE 3+. We do this by comparing the datasets for both the medium term for lead times of 4–9 years (Fig. 5). Although the LE analysis only includes 12 of the 42 GCMs that went into the MMLE 3+ linear model, we can get a sense of the consistency between the CMIP6 suite of GCMs. This informs our interpretation of the two dominant modes of variability, namely, the IPO and NINO34 with the LEs varying considerably for both modes of variability during both periods. Although the influence of the IPO and NINO34 are seen to gradually decrease over time for the MMLE 3+, the individual LEs show large

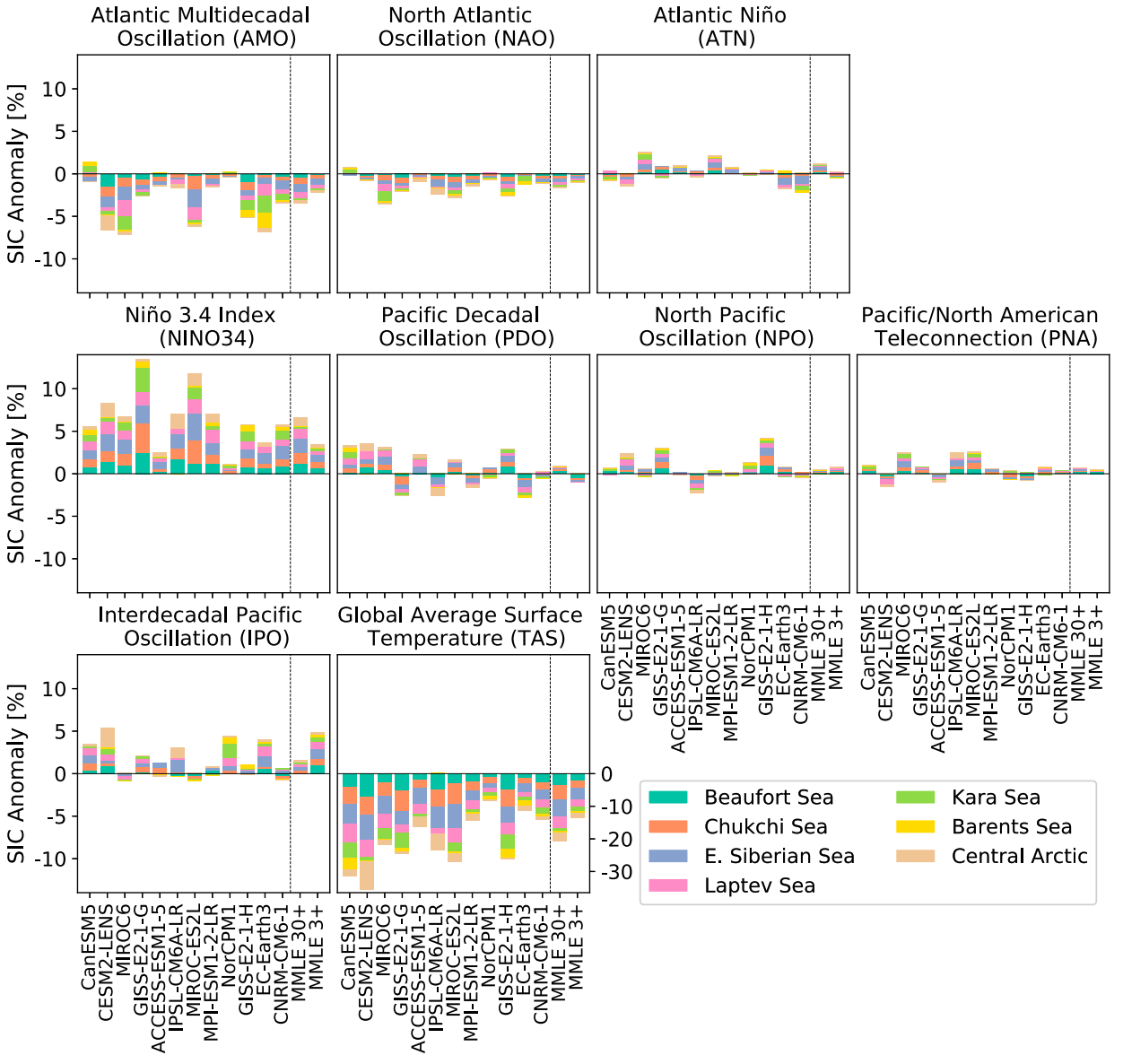

FIG. 5. The linear effect on regional SIC for 12 large ensembles and the two multimodel large ensembles. Linear response in September SIC for a +1 standard deviation anomaly of each climate mode, as in Fig. 4, but averaged over two distinct lead times. Bars are the linear response averaged over 4–9-yr lead times. Agreement within the CMIP6 suite of GCMs is high where bars are similar in magnitude and sign. Note the different *y*-axis scales for the global average surface temperature.

magnitudes of influence on SIC for both time periods, and the sign is inconsistent between LEs. We find little consensus across GCMs on the sign of the influence of the IPO across the 12 LEs. However, when we include these same 12 GCMs and 30 others in the MMLE 3+, a more positive signal emerges. This suggests either the additional 30 GCMs used in the MMLE 3+ have stronger positive linear relationships and/or that by chance, the first members used in the MMLE 3+ have a disproportionately strong positive relationship compared to the many members used for training in the LEs for a given GCM.

For the NINO34, there appears more consistency across the full CMIP6 suite of models with similarities between the collection of 12 LEs and both MMLEs. This again highlights the importance of taking a multimodel approach for the detection of low-frequency variability as two GCMs selected at random may produce vastly different results. Further, although we use large ensembles, the teleconnections between the tropics and the Arctic may vary considerably between realization within a large ensemble. Without pooling multiple GCMs and members, we may not be able to capture the full possible range of tropical–Arctic linkages which could be present over a 74-yr time period.

The AMO has a reasonably good agreement between the LEs with almost all indicating a negative influence on regional

SIC in the medium term. The PDO in the MMLE 3+ has near-zero influence; across all 12 Les, we can see that none indicate the PDO as being particularly influential, with disagreement in sign reducing the overall effect for the MMLE 3+. For the other modes of variability, we find that almost all of the LEs coefficients are small in magnitude and without overwhelming agreement on the sign. This allows us to interpret the MMLE 3+ near-zero coefficients as being representative of both the lack of consensus across CMIP6 GCMs and no strong relationships being found in any of the LEs.

The average magnitude of influence across all modes of variability differs considerably between individual LEs. For example, CESM2-LENS often produces the largest magnitudes for a given mode, and NorCPM1 often produces the smallest magnitudes for a given mode. Such systematic differences may occur due to differences in the mean state and magnitude of variability by GCM. This may well be the case considering the SIC anomaly is recorded in percentage points and CEMS2-LENS has a low biased summer mean state (DuVivier et al. 2020) and consequently large variability. Conversely, NorCPM1 has been noted as having a high-biased sea ice thickness (Bethke et al. 2021), which may explain why NorCPM1 is an outlier for small low-frequency SIC variability. Again, this indicates care must be taken to understand the effect of limitations on the results from individual LEs. Although many of the CMIP6 suite of GCMs are related (Knutti et al. 2013), and their biases may not average out, taking the results from the MMLE 3+ can reduce the risk of extreme outliers.

When testing our MMLE 3+ model on unseen members from the 42 GCMs, we find a large variation between GCMs and ensemble members (see Fig. 6). This limits our ability to determine which GCMs are most like the CMIP6 consensus if they have small ensemble sizes which cannot populate the full range of potential values (Notz 2015). Observational comparison with a similar time period will therefore be also difficult as observations could be expected, due to internal variability, to fall somewhere between 0 and 0.5 r^2 if internal variability in the actual climate system behaves similarly to the range of ensemble members in a large ensemble such as CanESM5.

Despite the ensemble member disagreement, the MMLE 3+ model appears to be well generalized to multiple GCMs as the test r^2 values appear very similar if a linear model is trained on all 42 GCMs as for the MMLE 3+ (blue circles in Fig. 6) or only on other members from the same GCM as for the LE (red triangles). CESM2-LENS has a wide distribution of test r^2 values between ensemble members, with larger variations between the microperturbations (atmospheric state) than between ensemble members with different ocean states (macroperturbations) (see Fig. S3), as also found for pan-Arctic sea ice volume variability (Kay et al. 2022). This indicates that for a 74-yr time period, the specific manifestation of the relationships between climate variability modes and regional Arctic SIC anomalies can be highly dependent on the the initial climate state.

e. Observational comparisons

Correlations between the climate modes and extreme SIC anomalies show observations broadly fall within what is simulated for the LEs, but validation is difficult due to the large differences between realizations. To directly compare observations with ensemble members, we compute the correlation between the six most extreme regional SIC anomaly years in the period 1956–2022 and correlate whether each mode of variability was in a positive or negative phase. To make a more representative sample, we pool the seven regions (except the Barents Sea where summer variability is near zero), averaged over a 4–9-yr lead time. However, the correlations should not be seen as comparable to the linear model as the correlations are binary, unlike the abilities of the linear model to apply lower weights to less important climate modes. Observations fall within the ensemble spread for all GCMs for all modes of variability except for the AMO which falls outside of only the NorCPM1, and the ATN and NPO which are outside multiple GCM ensemble ranges (see Fig. 7). This suggests that the observed correlations between most climate modes of variability and SIC anomalies are consistent with the CMIP6 large ensembles, within internal variability uncertainty. The far stronger correlation of observations for the ATN and NPO may mean that in our one realization of reality, these modes of variability have played a larger role than has been simulated in many climate models. Again, the large spread between realizations within a large ensemble highlights the extremely large range that observations would be expected to fall within (particularly for the IPO) and hence the difficulty of validating the simulated low-frequency drivers with observations.

f. Future projections

Our limited time period of observations may not be representative of a typical climate realization and therefore may arbitrarily match well or poorly to a specific machine learning model trained on GCMs. However, validation of our LE and MMLE 3+ models against the period 1956–2022 may have some implications for how well we can expect projections over the next 4–20 years to hold up. The r^2 values of the MMLE 3+ validated against the observations (Fig. 8 prediction columns) are similar to that of the MMLE 3+ validated against the second large ensemble members (Fig. 3). The MMLE 3+ and the best LEs, when used for hindcasting SIC anomalies from observed climate modes, often achieve r^2 values of between 0.2 and 0.3 above persistence but are highly regionally dependent. As the MMLE 3+ typically has the highest or near highest validation skill against the observations, we use these for future projections in the following.

For all regions of the Arctic, our linear model predicts below-trend sea ice concentrations over the coming decade. The seven regions have different time evolutions of the projected SIC anomalies; however, all regions for the MMLE 3+ projections show accelerated SIC loss due to low-frequency variability over the 20 years following 2022 (see Fig. 8). Taking the pan-Arctic as a whole, the predicted negative anomaly from the linear trend is the largest anomaly at a 5-yr lead time during the period 1956–2022. Therefore, our MMLE 3+ model predicts current climate modes as being particularly conducive to a large low-frequency SIC anomaly. This is fairly

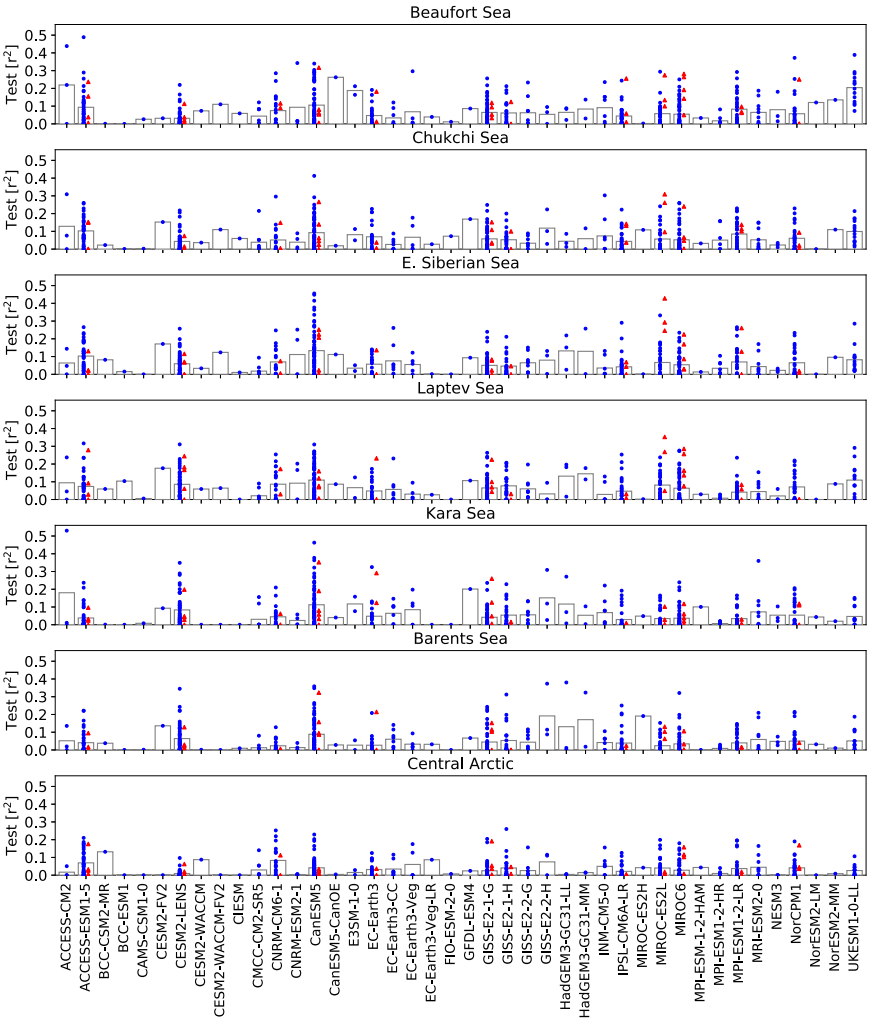

FIG. 6. September r^2 values for the test ensemble members from either the multimodel large ensemble (3+; blue) or the 12 single GCM large ensembles (red). The performance of the test members (third and later ensemble members) for the 42 GCMs included in the MMLE 3+ model are shown as blue circles, and ensemble mean values are indicated by gray bars. The red triangles indicate the performance of the test members for the individually trained linear models for each of the 12 LEs, where 10% of the LE members were reserved for testing against the linear model trained and validated on the first 75% and 15% of members from each GCM. Where the red triangles and blue circles for a given GCM have a similar distribution, the MMLE 3+ is equally good at capturing the relationships between climate modes and SIC as the LE, indicating the MMLE 3+ is well generalized. The r^2 values are for a 5-yr lead time minus persistence.

consistent across LEs, with the only large outlier being the CESM2-LENS which predicts an extreme accelerated loss due to being a large outlier in central Arctic projections. This outlier is likely due to thin biased ice as discussed in section 3d. Comparing the persistence of CESM2-LENS with CESM2-lessmelt runs which have thicker sea ice (Kay et al. 2022), the lessmelt CESM2 variant is more in line with the persistence in other GCMs (see Fig. S4). This indicates the low thickness bias likely caused the enhanced simulated variability outlier.

The contributions to this predicted accelerated SIC loss throughout the Arctic in the coming decade are dominated by the large anomalies in 2022 of a negative IPO and strongly positive AMO, alongside a moderately negative NINO34 value. Furthermore, the above-trend surface temperature warming in 2022 is also modeled as being a large contribution in the year 2027 (see Figs. 8q,r). Only the negative phase of the PDO in 2022 is expected to counter the accelerated sea ice loss by leading to positive SIC anomalies in the Pacific sector. The remaining modes of variability are either in a near-neutral phase in 2022 or have small influences on the linear model and hence do not feature as contributing to future anomalies. The alignment of modes of variability phases in 2022 combines to simulate a negative anomaly to the linear trend larger than any anomaly predicted during the period

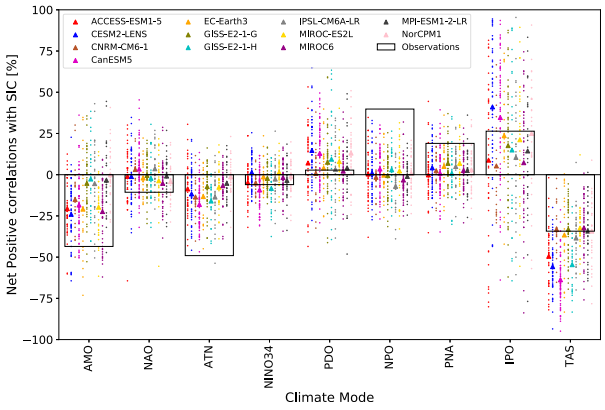

FIG. 7. Correlations between ensemble members and observations between modes of variability and extreme SIC anomaly events. The six most extreme SIC positive and negative anomalies are found for each ensemble member and September observations over the period 1956–2014. For a lead time of 4–9 years, the positive and negative correlations with each mode of variability are summed. These data are the average for the Beaufort, Chukchi, East Siberian, Kara, and Laptev Seas and the central Arctic. Each colored dot indicates the correlations for a single ensemble member, with the same colored triangle indicating the ensemble mean. The observed value for each variable is shown with a black hollow bar. When observations lie within a given GCM ensemble member distribution, the correlation in the observations is consistent with that simulated in the GCM.

1956–2021. Even if, for example, there were a sudden switch in phase of the Niño-3.4 index from −0.8 in 2022 to +2.0 standard deviations, the SIC percentage point influence in the East Siberian Sea would change the projected 2027 contribution from −0.78% to 1.89%. The more dominant modes of variability, namely, the IPO and AMO as well as the TAS, influence transition phase more slowly, which would therefore reduce the sensitivity of projections based on a single year.

4. Discussion

Skillful projections of regional Arctic SIC anomalies are able to be produced using simple linear relationships. This has allowed us to identify the individual impact of the dominant modes of variability, namely, the IPO, NINO34, and the AMO. However, covariance between the climate modes of variability and nonlinearities in their effect on sea ice are likely to exist (e.g., Heo et al. 2021). This is also supported by the fact that many of the climate modes of variability are not spatially or temporally independent of one another, such as the PDO and NINO34 (Chen and Wallace 2016). The lack of improvement in skill when we included nonlinearities or covariance in our analysis may be a result of a lack of data (see section 3a) despite the quantity and quality of GCM data available from CMIP6 simulations being unprecedented (Davy and Outten 2020). The multimodal ensemble approach to learning the drivers of Arctic sea ice variability did not degrade our skill when compared with training our linear model on a single GCM (see section 3d). This shows that a generalized model can be obtained from a variety of GCMs differing in model physics, model biases, and ocean states. However, large differences in validation between realizations indicate the extent to which the linear relationships themselves can differ due to internal variability.

Previous studies have primarily focused on seasonal or interannual time scales of variability, with the notable exceptions of the IPO and AMO which have been considered on decadal time scales. As these modes of variability persist in one phase for several years to decades, it is unsurprising for their influence on sea ice to also persist with a slow near-monotonic decay with time. We found the IPO to be the most influential mode of variability on all lead times between 4 and 20 years, positively correlated with SIC anomalies in all regions. In previous research, the IPO's influence on Arctic sea ice has not been featured, except as found by Screen and Deser (2019) for the CMIP5 GCM CESM1. The transition between the negative and positive IPO phase in CESM1 was found to be associated with a strengthened Aleutian low which enhances poleward heat and moisture transports, facilitating enhanced Arctic sea ice loss. The disagreement in sign and longevity of the IPO's influence on SIC between the CMIP6 LEs follows on from the research that CMIP5 GCMs generally poorly simulate the extratropical effects of the IPO (Baxter et al. 2019; Ding et al. 2019; Topál et al. 2020). In addition to the lack of consensus between GCMs broadly, the correlation appears highly sensitive to realization (see Fig. 7). Previous studies have suggested the variability in the strength of the Pacific–Arctic (PARC) teleconnection may cause the linkages between Pacific SST anomalies and Arctic sea ice to vary substantially and even change sign depending on initial climate state (Bonan and Blanchard-Wrigglesworth 2020). Additional focus on this mode with a wider variety of modeling applications appears needed and is particularly pressing given the strong current negative phase (see Fig. 8q).

The AMO was found in our MMLE 3+ linear model to be negatively correlated with all regions of the Arctic sea ice, which shows good agreement with previous studies (e.g., Day et al. 2012; Miles et al. 2014; Li et al. 2018b) for the pan-Arctic or Atlantic sector on decadal time scales. The suggested physical mechanism for a positive AMO leading to sea ice loss is the enhanced winter atmospheric heat transport into the Atlantic sector of the Arctic (Day et al. 2012). However, the AMO itself may have a forced component (Murphy et al. 2021; Cai et al. 2021; Klavans et al. 2022), and its oscillatory time scale varies considerably between GCMs (Lee et al. 2021), potentially limiting the use of the AMO as an independent variable. Despite this, the preindustrial control simulations (see Fig. S2) match well with the MMLE 3+ for 1920–2014 for the IPO and AMO, suggesting that forcing context is not highly important for these modes. A much smaller influence of the NINO34 in the preindustrial control simulations may suggest sensitivity to climate state. Similarly, the selection of the dominant season based on the LEs in the period 1920–2014 could also cause an array of responses in different climate conditions and for different GCMs if they simulate other seasons as being most influential.

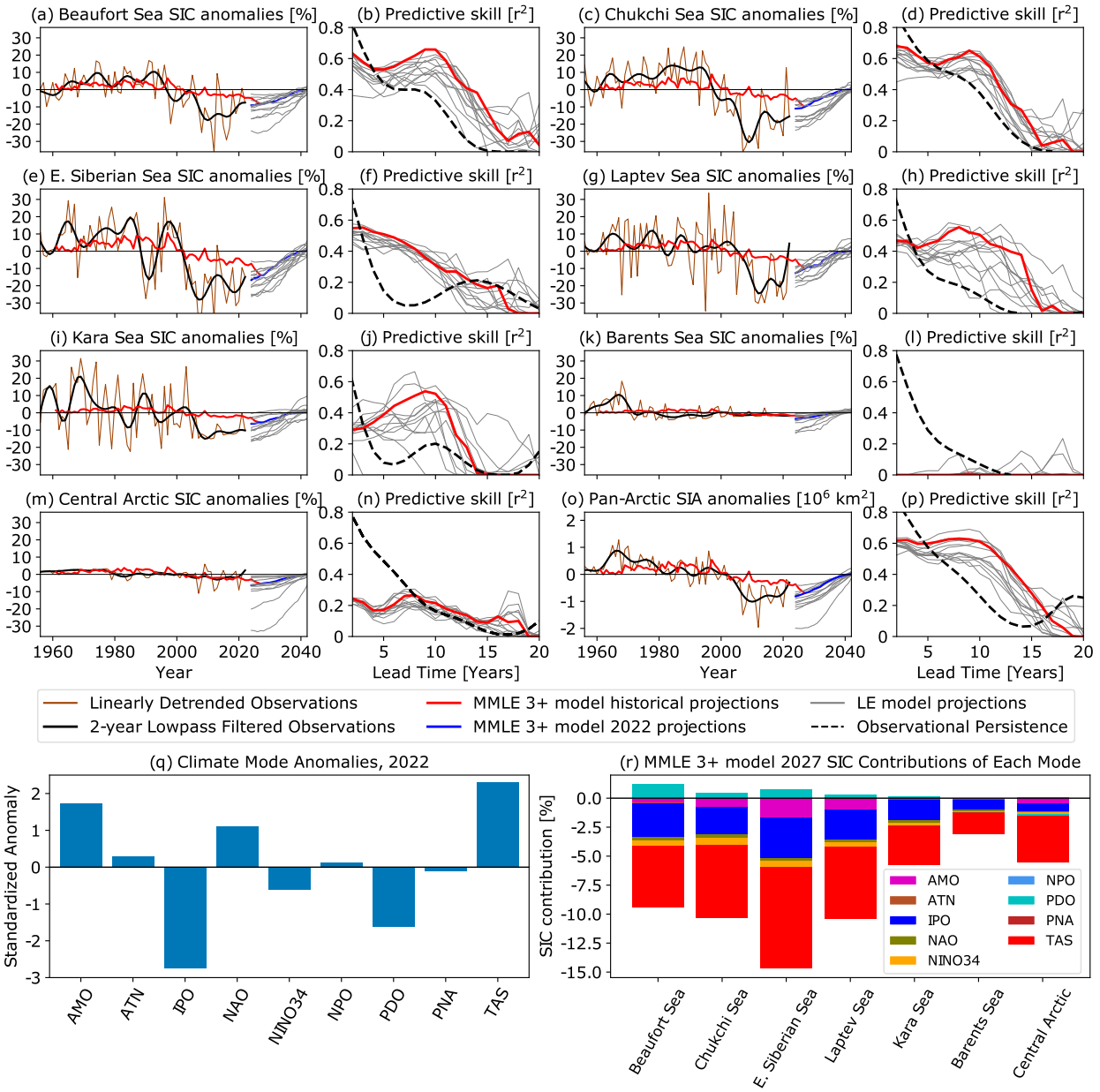

FIG. 8. Linear model projections of SIC anomalies based on observed climate modes. (a),(c),(e),(g),(i),(k),(m),(o) The observed 1956–2022 regional or pan-Arctic SIC anomalies (brown), the 2-yr low-pass-filtered anomalies (black), the MML3+ linear model historical hindcasts on a 5-yr lead time (red), the future projections based on the climate mode anomalies observed in 2022 using the MMLE 3+ (blue), and individual LEs (gray). (b),(d),(f),(h),(j),(l),(n),(p) The observed persistence in dashed back lines, while the MMLE 3+ and LE hindcast performances for 1976–2022 at 2–20-yr lead times are shown in red and gray, respectively. (q) The observed climate mode anomalies for the year 2022. (r) The MMLE 3+ contribution to the projected anomalies in 2027 based on 2022 data of each of the modes of variability.

El Niño and La Niña have been shown to be influential on Arctic sea ice and generally suggest that NINO34 is positively correlated with SIC except for the Beaufort Sea (e.g., Clancy et al. 2021; Hu et al. 2016; Jeong et al. 2022b). However, the lead times considered previously were shorter than our 4–20-yr time scale, making our positively correlated influence hard to directly compare with previous research. Furthermore, previous studies on shorter time scales have noted the importance of the type of El Niño regime (Jeong et al. 2022a; Lee et al. 2023) and the likely nonlinear and asymmetrical climate response from NINO34 variations (Hoerling et al. 1997). Limitations to the detection of lagged influence from ENSO could be derived from the fact that CMIP6 GCMs still fail to accurately simulate the periodicity and phase-locking characteristics of ENSO (Hou and Tang 2022). Nonetheless, El Niño favoring a positive Arctic Oscillation and a deepened

Aleutian low via Rossby wave trains, which in turn promote enhanced sea ice export, have been shown to exist in a number of CMIP5 and CMIP6 GCMs (Clancy et al. 2021; Lee et al. 2023). What remains elusive is the persistence of the influence of the NINO34 on sea ice across GCMs up to approximately 14 years (Fig. 4). This is surprising due to the transition between phases often occurring interannually, which would therefore require persistent lagged teleconnection pathway to the Arctic which has not been suggested. During 1970–2014 when radiative forcing increase was more linear compared with 1920–2014, we found NINO34 still has a positive correlation on sea ice but only for approximately 5 years (Fig. S1). For preindustrial control simulations, a constant near-zero relationship was found (Fig. S2). It would therefore appear that for periods when nonlinearities in radiative forcing are more effectively removed by detrending or by constant forcing, the lagged NINO34 influence on sea ice is substantially reduced. As no physical mechanism for a lagged sea ice response to a given phase of NINO34 is suggested, the influence of NINO34 encapsulating residuals in the model or nonlinearities in warming must be considered.

The PDO was previously not found to be highly important for Arctic sea ice by itself (Zhang et al. 2020; Karami et al. 2023), and its influence may also have changed over time (Bonan and Blanchard-Wrigglesworth 2020; Kim et al. 2020). Similarly, we also only found a small influence of the PDO over our long time period of 1920–2014. The SST pattern of the PDO is related to the Pacific SST climate modes of the NINO34 and IPO, which each have similar teleconnection mechanisms via Rossby wave train formation (Yuan et al. 2018). Further, the mechanisms of an oceanic "tunnel" and atmospheric "bridge" may be common between the IPO and PDO, leading to similar characteristics of persistence, Arctic influence, and modulation by ENSO (Liu and Alexander 2007; Henley et al. 2017). Therefore, it is unsurprising for a subset of tropical Pacific modes of variability to dominate due to their similarity. The ATN is the only negligible mode of variability derived from SSTs but has not previously been identified as the specific driver of Arctic sea ice variability. However, the tropical Atlantic has been suggested to influence Arctic sea ice (Meehl et al. 2018). Thus, the unimportant nature of the ATN does not preclude other aspects of the tropical Atlantic from being important.

Consistent with the previous lack of evidence of influence beyond interannual time scales, the sea level pressure–derived modes of variability (the NAO, NPO, and PNA) were found to have negligible effect at lead times of 4–20 years. Previous research has shown the effect of the NAO to decay to zero after approximately 2 years (Ukita et al. 2007); this time scale and the regional correlations (e.g., Serreze et al. 2007; Döscher et al. 2010) align with our findings given the smoothing inherent in our low-pass-filtered data. This provides confidence in our linear model's ability to capture higher-frequency variability but dismiss low-frequency influence from these modes of variability.

5. Conclusions

We have shown that low-frequency variability of regional Arctic sea ice concentration can be modeled using linear drivers consisting of climate modes of variability. We achieve predictions superior to persistence for most regions for a lead time of 4–20 years and find that the climate modes of variability can be considered independently without reducing skill. By comparing the linear responses between 12 large ensembles from CMIP6 and a multimodel large ensemble comprising 42 GCMs, we find where there is consensus of the dominant linear drivers of low-frequency sea ice variability except in the case of the IPO. In the pan-Arctic, we are able to explain up to 60% of observed low-frequency sea ice concentration variability at lead times of 5 years. However, the ability of a GCM or a multimodel large ensemble to predict unseen ensemble members or observations can vary wildly depending on the realization of internal variability; between 0 and 0.46 r^2 in the case of CanESM5, the largest single GCM ensemble. Hence, both of these complicate the analysis of small samples of GCMs and the application and verification of these relationships with our single realization of observations.

The most important modes of variability we found were the IPO, NINO34, and the AMO. The multimodel large ensemble linear model showed the IPO to have a strong positive correlation with this being most pronounced in the East Siberian, Beaufort, and Laptev Seas at lead times of up to 14 years. Although this large magnitude of influence of the IPO was found across GCMs, the sign and regional influence was especially dependent on the GCM used and the specific realization of internal variability. NINO34 was found to be positively correlated with SIC anomalies in all regions, particularly in the Pacific sector. This correlation was more consistent between GCMs, with disagreement growing at longer lead times. The AMO was the only other mode of variability considered important for long periods of time, being modeled as highly negatively correlated with SIC across all regions for up to approximately 10 years. However, the agreement across CMIP6 GCMs for the AMO was less consistent than NINO34. The persistence of influence on sea ice from the IPO and AMO is not surprising due to their similar phase persistence. NINO34 in contrast can change phase interannually, suggesting the influence found here may be an artifact of forcing conditions, as no physical mechanism for a delayed Arctic influence has been suggested.

When using our linear model to make predictions, we find a near "perfect storm" of modes of variability in the year 2021/22 to induce acceleration to the sea ice loss trend over the next decade. The primary influences of this projected acceleration of low-frequency variability-driven sea ice loss are an above-trend global average surface temperature warming, a negative IPO, La Niña conditions, and a positive AMO. For the pan-Arctic, the projected low-frequency deviation from the long-term trend due to current climate mode phase configurations is expected to be the largest since at least 1956. While the transition between La Niña and El Niño can occur rapidly, the fact that our strong negative predictions are primarily due to the slowly changing climate modes of the AMO and IPO implies the robustness of this prediction to interannual variability. Of course, the sea ice anomalies that will actually be observed are still dominated by interannual variability, which makes up roughly three-quarters of the total variability. Thus, while we cannot say with confidence that a new record low

September extent will occur over the next decade, the modeled low-frequency variability suggests that extremely low SIC values will be more likely over the coming decade, with low-frequency variability likely to enhance the long-term negative trend.

Acknowledgments. This work was supported by the National Science Foundation under Grant 1847398. A. Jahn's contribution was also supported by an Alexander von Humboldt fellowship. We would also like to acknowledge high-performance computing on Cheyenne (https://doi.org/10.5065/D6RX99HX) provided by NCAR's Computational and Information Systems Laboratory, sponsored by the National Science Foundation. Further, we thank Adam Philips for processing updates to the Climate Variability Diagnostics Package output used in this analysis. We also thank Elizabeth Barnes and David Hall for useful conversations in the early part of the project.

Data availability statement. The data used in this study are freely available at https://esgf-node.llnl.gov/projects/cmip6/ for the CMIP6 global climate model data except for the CESM2-LENS, which is available at https://www.cesm.ucar.edu/community-projects/lens2/data-sets. The CVDP data are available at https://www.cesm.ucar.edu/projects/cvdp/data-repository. The observational sea ice concentration data are freely available at https://www.metoffice.gov.uk/hadobs/hadisst/data/download.html. All code required to replicate this study has been made open-access via Zenodo at https://doi.org/10.5281/zenodo.12580233. Additionally, the linear model coefficients and validation statistics can be accessed from the Arctic Data Center at https://doi.org/10.18739/A2MS3K35M.

REFERENCES

Alexander, M. A., I. Bladé, M. Newman, J. R. Lanzante, N.-C. Lau, and J. D. Scott, 2002: The atmospheric bridge: The influence of ENSO teleconnections on air–sea interaction over the global oceans. *J. Climate*, **15**, 2205–2231, https://doi.org/10.1175/1520-0442(2002)015<2205:TABTIO>2.0.CO;2.

Årthun, M., I. H. Onarheim, J. Dörr, and T. Eldevik, 2021: The seasonal and regional transition to an ice-free Arctic. *Geophys. Res. Lett.*, **48**, e2020GL090825, https://doi.org/10.1029/2020GL090825.

Bader, D. C., R. Leung, M. Taylor, and R. B. McCoy, 2019: E3SM-Project E3SM1.0 model output prepared for CMIP6 CMIP historical. Earth System Grid Federation, accessed 25 January 2023, https://doi.org/10.22033/ESGF/CMIP6.4497.

Barnes, E. A., J. W. Hurrell, I. Ebert-Uphoff, C. Anderson, and D. Anderson, 2019: Viewing forced climate patterns through an AI lens. *Geophys. Res. Lett.*, **46**, 13 389–13 398, https://doi.org/10.1029/2019GL084944.

Barnhart, K. R., C. R. Miller, I. Overeem, and J. E. Kay, 2016: Mapping the future expansion of Arctic open water. *Nat. Climate Change*, **6**, 280–285, https://doi.org/10.1038/nclimate2848.

Baxter, I., and Coauthors, 2019: How tropical Pacific surface cooling contributed to accelerated sea ice melt from 2007 to 2012 as ice is thinned by anthropogenic forcing. *J. Climate*, **32**, 8583–8602, https://doi.org/10.1175/JCLI-D-18-0783.1.

Bentsen, M., and Coauthors, 2019: NCC NorESM2-MM model output prepared for CMIP6 CMIP historical. Earth System Grid Federation, accessed 25 January 2023, https://doi.org/10.22033/ESGF/CMIP6.8040.

Bethke, I., and Coauthors, 2019: NCC NorCPM1 model output prepared for CMIP6 CMIP historical. Earth System Grid Federation, accessed 25 January 2023, https://doi.org/10.22033/ESGF/CMIP6.10894.

——, and Coauthors, 2021: NorCPM1 and its contribution to CMIP6 DCPP. *Geosci. Model Dev.*, **14**, 7073–7116, https://doi.org/10.5194/gmd-14-7073-2021.

Blanchard-Wrigglesworth, E., and M. Bushuk, 2019: Robustness of Arctic sea-ice predictability in GCMs. *Climate Dyn.*, **52**, 5555–5566, https://doi.org/10.1007/s00382-018-4461-3.

——, K. C. Armour, C. M. Bitz, and E. DeWeaver, 2011: Persistence and inherent predictability of Arctic sea ice in a GCM ensemble and observations. *J. Climate*, **24**, 231–250, https://doi.org/10.1175/2010JCLI3775.1.

Bonan, D. B., and E. Blanchard-Wrigglesworth, 2020: Nonstationary teleconnection between the Pacific Ocean and Arctic sea ice. *Geophys. Res. Lett.*, **47**, e2019GL085666, https://doi.org/10.1029/2019GL085666.

——, M. Bushuk, and M. Winton, 2019: A spring barrier for regional predictions of summer Arctic sea ice. *Geophys. Res. Lett.*, **46**, 5937–5947, https://doi.org/10.1029/2019GL082947.

——, F. Lehner, and M. M. Holland, 2021: Partitioning uncertainty in projections of Arctic sea ice. *Environ. Res. Lett.*, **16**, 044002, https://doi.org/10.1088/1748-9326/abe0ec.

Boucher, O., and Coauthors, 2018: IPSL IPSL-CM6A-LR model output prepared for CMIP6 CMIP historical. Earth System Grid Federation, accessed 25 January 2023, https://doi.org/10.22033/ESGF/CMIP6.5195.

Brown, J. R., and Coauthors, 2020: Comparison of past and future simulations of ENSO in CMIP5/PMIP3 and CMIP6/PMIP4 models. *Climate Past*, **16**, 1777–1805, https://doi.org/10.5194/cp-16-1777-2020.

Bushuk, M., and D. Giannakis, 2017: The seasonality and interannual variability of Arctic Sea ice reemergence. *J. Climate*, **30**, 4657–4676, https://doi.org/10.1175/JCLI-D-16-0549.1.

——, R. Msadek, M. Winton, G. Vecchi, X. Yang, A. Rosati, and R. Gudgel, 2019: Regional Arctic sea–ice prediction: Potential versus operational seasonal forecast skill. *Climate Dyn.*, **52**, 2721–2743, https://doi.org/10.1007/s00382-018-4288-y.

Cai, Q., D. Beletsky, J. Wang, and R. Lei, 2021: Interannual and decadal variability of Arctic summer sea ice associated with atmospheric teleconnection patterns during 1850–2017. *J. Climate*, **34**, 9931–9955, https://doi.org/10.1175/JCLI-D-20-0330.1.

Cao, J., and B. Wang, 2019: NUIST NESMv3 model output prepared for CMIP6 CMIP historical. Earth System Grid Federation, accessed 25 January 2023, https://doi.org/10.22033/ESGF/CMIP6.8769.

Chen, X., and J. M. Wallace, 2016: Orthogonal PDO and ENSO indices. *J. Climate*, **29**, 3883–3892, https://doi.org/10.1175/JCLI-D-15-0684.1.

Clancy, R., C. Bitz, and E. Blanchard-Wrigglesworth, 2021: The influence of ENSO on Arctic sea ice in large ensembles and observations. *J. Climate*, **34**, 9585–9604, https://doi.org/10.1175/JCLI-D-20-0958.1.

Crawford, A., J. Stroeve, A. Smith, and A. Jahn, 2021: Arctic open-water periods are projected to lengthen dramatically by 2100. *Commun. Earth Environ.*, **2**, 109, https://doi.org/10.1038/s43247-021-00183-x.

Dalelane, C., K. Winderlich, and A. Walter, 2023: Evaluation of global teleconnections in CMIP6 climate projections using complex networks. *Earth Syst. Dyn.*, **14**, 17–37, https://doi.org/10.5194/esd-14-17-2023.

Danabasoglu, G., 2019a: NCAR CESM2-FV2 model output prepared for CMIP6 CMIP historical. Earth System Grid Federation, accessed 25 January 2023, https://doi.org/10.22033/ESGF/CMIP6.11297.

——, 2019b: NCAR CESM2 model output prepared for CMIP6 CMIP historical. Earth System Grid Federation, accessed 25 January 2023, https://doi.org/10.22033/ESGF/CMIP6.7627.

——, 2019c: NCAR CESM2-WACCM-FV2 model output prepared for CMIP6 CMIP historical. Earth System Grid Federation, accessed 25 January 2023, https://doi.org/10.22033/ESGF/CMIP6.11298.

——, 2019d: NCAR CESM2-WACCM model output prepared for CMIP6 CMIP historical. Earth System Grid Federation, accessed 25 January 2023, https://doi.org/10.22033/ESGF/CMIP6.10071.

Davy, R., and S. Outten, 2020: The Arctic surface climate in CMIP6: Status and developments since CMIP5. *J. Climate*, **33**, 8047–8068, https://doi.org/10.1175/JCLI-D-19-0990.1.

Day, J. J., J. C. Hargreaves, J. D. Annan, and A. Abe-Ouchi, 2012: Sources of multi-decadal variability in Arctic sea ice extent. *Environ. Res. Lett.*, **7**, 034011, https://doi.org/10.1088/1748-9326/7/3/034011.

——, E. Hawkins, and S. Tietsche, 2014: Will Arctic sea ice thickness initialization improve seasonal forecast skill? *Geophys. Res. Lett.*, **41**, 7566–7575, https://doi.org/10.1002/2014GL061694.

Deser, C., and Coauthors, 2020: Insights from Earth system model initial-condition large ensembles and future prospects. *Nat. Climate Change*, **10**, 277–286, https://doi.org/10.1038/s41558-020-0731-2.

Diffenbaugh, N. S., and E. A. Barnes, 2023: Data-driven predictions of the time remaining until critical global warming thresholds are reached. *Proc. Natl. Acad. Sci. USA*, **120**, e2207183120, https://doi.org/10.1073/pnas.2207183120.

Ding, Q., and Coauthors, 2019: Fingerprints of internal drivers of Arctic sea ice loss in observations and model simulations. *Nat. Geosci.*, **12**, 28–33, https://doi.org/10.1038/s41561-018-0256-8.

Dix, M., and Coauthors, 2019: CSIRO-ARCCSS ACCESS-CM2 model output prepared for CMIP6 CMIP historical. Earth System Grid Federation, accessed 25 January 2023, https://doi.org/10.22033/ESGF/CMIP6.4271.

Docquier, D., T. Koenigk, R. Fuentes-Franco, M. P. Karami, and Y. Ruprich-Robert, 2021: Impact of ocean heat transport on the Arctic sea-ice decline: A model study with EC-Earth3. *Climate Dyn.*, **56**, 1407–1432, https://doi.org/10.1007/s00382-020-05540-8.

Dörr, J. S., D. B. Bonan, M. Årthun, L. Svendsen, and R. C. J. Wills, 2023: Forced and internal components of observed Arctic sea-ice changes. *Cryosphere*, **17**, 4133–4153, https://doi.org/10.5194/tc-17-4133-2023.

Döscher, R., K. Wyser, H. E. Meier, M. Qian, and R. Redler, 2010: Quantifying Arctic contributions to climate predictability in a regional coupled ocean-ice-atmosphere model. *Climate Dyn.*, **34**, 1157–1176, https://doi.org/10.1007/s00382-009-0567-y.

DuVivier, A. K., M. M. Holland, J. E. Kay, S. Tilmes, A. Gettelman, and D. A. Bailey, 2020: Arctic and Antarctic sea ice mean state in the Community Earth System Model version 2 and the influence of atmospheric chemistry. *J. Geophys. Res. Oceans*, **125**, e2019JC015934, https://doi.org/10.1029/2019JC015934.

EC-Earth-Consortium, 2019a: EC-Earth-Consortium EC-Earth3 model output prepared for CMIP6 CMIP historical. Earth System Grid Federation, accessed 25 January 2023, https://doi.org/10.22033/ESGF/CMIP6.4700.

——, 2019b: EC-Earth-Consortium EC-Earth3-Veg model output prepared for CMIP6 CMIP historical. Earth System Grid Federation, accessed 25 January 2023, https://doi.org/10.22033/ESGF/CMIP6.4706.

——, 2020: EC-Earth-Consortium EC-Earth3-Veg-LR model output prepared for CMIP6 CMIP historical. Earth System Grid Federation, accessed 25 January 2023, https://doi.org/10.22033/ESGF/CMIP6.4707.

——, 2021: EC-Earth-Consortium EC-Earth-3-CC model output prepared for CMIP6 CMIP historical. Earth System Grid Federation, accessed 25 January 2023, https://doi.org/10.22033/ESGF/CMIP6.4702.

Eguíluz, V. M., J. Fernández-Gracia, X. Irigoien, and C. M. Duarte, 2016: A quantitative assessment of Arctic shipping in 2010–2014. *Sci. Rep.*, **6**, 30682, https://doi.org/10.1038/srep30682.

Eisenman, I., 2010: Geographic muting of changes in the Arctic sea ice cover. *Geophys. Res. Lett.*, **37**, L16501, https://doi.org/10.1029/2010GL043741.

England, M., A. Jahn, and L. Polvani, 2019: Nonuniform contribution of internal variability to recent Arctic sea ice loss. *J. Climate*, **32**, 4039–4053, https://doi.org/10.1175/JCLI-D-18-0864.1.

Fasullo, J. T., A. S. Phillips, and C. Deser, 2020: Evaluation of leading modes of climate variability in the CMIP archives. *J. Climate*, **33**, 5527–5545, https://doi.org/10.1175/JCLI-D-19-1024.1.

Fetterer, F., M. Savoie, S. Helfrich, and P. Clemente-Colón, 2010: Multisensor Analyzed Sea Ice Extent – Northern Hemisphere (MASIE-NH), version 1. U.S. National Ice Center and National Snow and Ice Data Center, accessed 9 March 2023, https://doi.org/10.7265/N5GT5K3K.

Francis, J. A., and B. Wu, 2020: Why has no new record-minimum Arctic sea-ice extent occurred since September 2012? *Environ. Res. Lett.*, **15**, 114034, https://doi.org/10.1088/1748-9326/abc047.

Furtado, J. C., E. Di Lorenzo, B. T. Anderson, and N. Schneider, 2012: Linkages between the North Pacific Oscillation and central tropical Pacific SSTs at low frequencies. *Climate Dyn.*, **39**, 2883–2846, https://doi.org/10.1007/s00382-011-1245-4.

Giesse, C., D. Notz, and J. Baehr, 2021: On the origin of discrepancies between observed and simulated memory of Arctic sea ice. *Geophys. Res. Lett.*, **48**, e2020GL091784, https://doi.org/10.1029/2020GL091784.

Goosse, H., O. Arzel, C. M. Bitz, A. de Montety, and M. Vancoppenolle, 2009: Increased variability of the Arctic summer ice extent in a warmer climate. *Geophys. Res. Lett.*, **36**, L23702, https://doi.org/10.1029/2009GL040546.

Gregory, W., J. Stroeve, and M. Tsamados, 2022: Network connectivity between the winter Arctic Oscillation and summer sea ice in CMIP6 models and observations. *Cryosphere*, **16**, 1653–1673, https://doi.org/10.5194/tc-16-1653-2022.

Guemas, V., and Coauthors, 2016: A review on Arctic sea-ice predictability and prediction on seasonal to decadal time-scales. *Quart. J. Roy. Meteor. Soc.*, **142**, 546–561, https://doi.org/10.1002/qj.2401.

Hajima, T., and Coauthors, 2019: MIROC MIROC-ES2L model output prepared for CMIP6 CMIP historical. Earth System

Grid Federation, accessed 25 January 2023, https://doi.org/10.22033/ESGF/CMIP6.5602.

Henley, B. J., and Coauthors, 2017: Spatial and temporal agreement in climate model simulations of the Interdecadal Pacific Oscillation. *Environ. Res. Lett.*, **12**, 044011, https://doi.org/10.1088/1748-9326/aa5cc8.

Heo, E.-S., M.-K. Sung, S.-I. An, and Y.-M. Yang, 2021: Decadal phase shift of summertime Arctic dipole pattern and its nonlinear effect on sea ice extent. *Int. J. Climatol.*, **41**, 4732–4742, https://doi.org/10.1002/joc.7097.

Hoerling, M. P., A. Kumar, and M. Zhong, 1997: El Niño, La Niña, and the nonlinearity of their teleconnections. *J. Climate*, **10**, 1769–1786, https://doi.org/10.1175/1520-0442(1997)010<1769:ENOLNA>2.0.CO;2.

Hofsteenge, M. G., R. G. Graversen, J. H. Rydsaa, and Z. Rey, 2022: The impact of atmospheric Rossby waves and cyclones on the Arctic sea ice variability. *Climate Dyn.*, **59**, 579–594, https://doi.org/10.1007/s00382-022-06145-z.

Holland, M. M., L. Landrum, D. Bailey, and S. Vavrus, 2019: Changing seasonal predictability of Arctic summer sea ice area in a warming climate. *J. Climate*, **32**, 4963–4979, https://doi.org/10.1175/JCLI-D-19-0034.1.

Hou, M., and Y. Tang, 2022: Recent progress in simulating two types of ENSO – From CMIP5 to CMIP6. *Front. Mar. Sci.*, **9**, 986780, https://doi.org/10.3389/fmars.2022.986780.

Hu, C., S. Yang, Q. Wu, Z. Li, J. Chen, K. Deng, T. Zhang, and C. Zhang, 2016: Shifting El Niño inhibits summer Arctic warming and Arctic sea-ice melting over the Canada Basin. *Nat. Commun.*, **7**, 11721, https://doi.org/10.1038/ncomms11721.

Huang, W., 2019: THU CIESM model output prepared for CMIP6 CMIP historical. Earth System Grid Federation, accessed 25 January 2023, https://doi.org/10.22033/ESGF/CMIP6.8843.

Hurrell, J. W., and C. Deser, 2009: North Atlantic climate variability: The role of the North Atlantic Oscillation. *J. Mar. Syst.*, **78**, 28–41, https://doi.org/10.1016/j.jmarsys.2008.11.026.

Jahn, A., 2018: Reduced probability of ice-free summers for 1.5°C compared to 2°C warming. *Nat. Climate Change*, **8**, 409–413, https://doi.org/10.1038/s41558-018-0127-8.

Jeong, H., H.-S. Park, M. F. Stuecker, and S.-W. Yeh, 2022a: Distinct impacts of major El Niño events on Arctic temperatures due to differences in eastern tropical Pacific sea surface temperatures. *Sci. Adv.*, **8**, eabl8278, https://doi.org/10.1126/sciadv.abl8278.

——, ——, ——, and ——, 2022b: Record low Arctic sea ice extent in 2012 linked to two-year La Niña-driven sea surface temperature pattern. *Geophys. Res. Lett.*, **49**, e2022GL098385, https://doi.org/10.1029/2022GL098385.

Kalnay, E., and Coauthors, 1996: The NCEP/NCAR 40-year reanalysis project. *Bull. Amer. Meteor. Soc.*, **77**, 437–472, https://doi.org/10.1175/1520-0477(1996)077<0437:TNYRP>2.0.CO;2.

Karami, M. P., T. Koenigk, and B. Tremblay, 2023: Variability modes of September Arctic sea ice: Drivers and their contributions to sea ice trend and extremes. *Environ. Res.: Climate*, **2**, 025005, https://doi.org/10.1088/2752-5295/accbe3.

Kay, J. E., M. M. Holland, and A. Jahn, 2011: Inter-annual to multi-decadal Arctic sea ice extent trends in a warming world. *Geophys. Res. Lett.*, **38**, L15708, https://doi.org/10.1029/2011GL048008.

——, and Coauthors, 2022: Less surface sea ice melt in the CESM2 improves Arctic sea ice simulation with minimal non-polar climate impacts. *J. Adv. Model. Earth Syst.*, **14**, e2021MS002679, https://doi.org/10.1029/2021MS002679.

Kim, H., S.-W. Yeh, S.-I. An, and S.-Y. Song, 2020: Changes in the role of Pacific decadal oscillation on sea ice extent variability across the mid-1990s. *Sci. Rep.*, **10**, 17564, https://doi.org/10.1038/s41598-020-74260-0.

Klavans, J. M., M. A. Cane, A. C. Clement, and L. N. Murphy, 2021: NAO predictability from external forcing in the late 20th century. *npj Climate Atmos. Sci.*, **4**, 22, https://doi.org/10.1038/s41612-021-00177-8.

——, A. C. Clement, M. A. Cane, and L. N. Murphy, 2022: The evolving role of external forcing in North Atlantic SST variability over the last millennium. *J. Climate*, **35**, 2741–2754, https://doi.org/10.1175/JCLI-D-21-0338.1.

Knutti, R., D. Masson, and A. Gettelman, 2013: Climate model genealogy: Generation CMIP5 and how we got there. *Geophys. Res. Lett.*, **40**, 1194–1199, https://doi.org/10.1002/grl.50256.

Kovacs, K. M., C. Lydersen, J. E. Overland, and S. E. Moore, 2011: Impacts of changing sea-ice conditions on Arctic marine mammals. *Mar. Biodiversity*, **41**, 181–194, https://doi.org/10.1007/s12526-010-0061-0.

Krasting, J. P., and Coauthors, 2018: NOAA-GFDL GFDL-ESM4 model output prepared for CMIP6 CMIP historical. Earth System Grid Federation, accessed 25 January 2023, https://doi.org/10.22033/ESGF/CMIP6.8597.

Kwok, R., and D. A. Rothrock, 2009: Decline in Arctic sea ice thickness from submarine and ICESat records: 1958–2008. *Geophys. Res. Lett.*, **36**, L15501, https://doi.org/10.1029/2009GL039035.

Labe, Z. M., and E. A. Barnes, 2022: Comparison of climate model large ensembles with observations in the Arctic using simple neural networks. *Earth Space Sci.*, **9**, e2022EA002348, https://doi.org/10.1029/2022EA002348.

Leathers, D. J., B. Yarnal, and M. A. Palecki, 1991: The Pacific/North American teleconnection pattern and United States climate. Part I: Regional temperature and precipitation associations. *J. Climate*, **4**, 517–528, https://doi.org/10.1175/1520-0442(1991)004<0517:TPATPA>2.0.CO;2.

Lee, J., K. R. Sperber, P. J. Gleckler, K. E. Taylor, and C. J. W. Bonfils, 2021: Benchmarking performance changes in the simulation of extratropical modes of variability across CMIP generations. *J. Climate*, **34**, 6945–6969, https://doi.org/10.1175/JCLI-D-20-0832.1.

Lee, S., H.-S. Park, S.-Y. Song, and S.-W. Yeh, 2023: Distinct impacts of two types of El Niño events on northern winter high-latitude temperatures simulated by CMIP6 climate models. *Environ. Res. Lett.*, **18**, 034035, https://doi.org/10.1088/1748-9326/acbce9.

Lenssen, N. J. L., G. A. Schmidt, J. E. Hansen, M. J. Menne, A. Persin, R. Ruedy, and D. Zyss, 2019: Improvements in the GISTEMP uncertainty model. *J. Geophys. Res. Atmos.*, **124**, 6307–6326, https://doi.org/10.1029/2018JD029522.

L'Heureux, M. L., A. Kumar, G. D. Bell, M. S. Halpert, and R. W. Higgins, 2008: Role of the Pacific-North American (PNA) pattern in the 2007 Arctic sea ice decline. *Geophys. Res. Lett.*, **35**, L20701, https://doi.org/10.1029/2008GL035205.

Li, D., R. Zhang, and T. Knutson, 2018a: Comparison of mechanisms for low-frequency variability of summer Arctic sea ice in three coupled models. *J. Climate*, **31**, 1205–1226, https://doi.org/10.1175/JCLI-D-16-0617.1.

Li, F., Y. J. Orsolini, H. Wang, Y. Gao, and S. He, 2018b: Atlantic multidecadal oscillation modulates the impacts of Arctic sea ice decline. *Geophys. Res. Lett.*, **45**, 2497–2506, https://doi.org/10.1002/2017GL076210.

Lindsay, R. W., and J. Zhang, 2006: Arctic ocean ice thickness: Modes of variability and the best locations from which to monitor them. *J. Phys. Oceanogr.*, **36**, 496–506, https://doi.org/10.1175/JPO2861.1.

Liu, Z., and M. Alexander, 2007: Atmospheric bridge, oceanic tunnel, and global climatic teleconnections. *Rev. Geophys.*, **45**, RG2005, https://doi.org/10.1029/2005RG000172.

——, and Coauthors, 2021: Acceleration of western Arctic sea ice loss linked to the Pacific North American pattern. *Nat. Commun.*, **12**, 1519, https://doi.org/10.1038/s41467-021-21830-z.

Long, M., L. Zhang, S. Hu, and S. Qian, 2021: Multi-aspect assessment of CMIP6 models for Arctic sea ice simulation. *J. Climate*, **34**, 1515–1529, https://doi.org/10.1175/JCLI-D-20-0522.1.

Lovato, T., and D. Peano, 2020: CMCC CMCC-CM2-SR5 model output prepared for CMIP6 CMIP historical. Earth System Grid Federation, accessed 25 January 2023, https://doi.org/10.22033/ESGF/CMIP6.3825.

MacDonald, G. M., and R. A. Case, 2005: Variations in the Pacific decadal oscillation over the past millennium. *Geophys. Res. Lett.*, **32**, L08703, https://doi.org/10.1029/2005GL022478.

Mantua, N. J., S. R. Hare, Y. Zhang, J. M. Wallace, and R. C. Francis, 1997: A Pacific interdecadal climate oscillation with impacts on salmon production. *Bull. Amer. Meteor. Soc.*, **78**, 1069–1080, https://doi.org/10.1175/1520-0477(1997)078<1069:APICOW>2.0.CO;2.

McBride, L. A., A. P. Hope, T. P. Canty, B. F. Bennett, W. R. Tribett, and R. J. Salawitch, 2021: Comparison of CMIP6 historical climate simulations and future projected warming to an empirical model of global climate. *Earth Syst. Dyn.*, **12**, 545–579, https://doi.org/10.5194/esd-12-545-2021.

Meehl, G. A., A. Hu, J. M. Arblaster, J. Fasullo, and K. E. Trenberth, 2013: Externally forced and internally generated decadal climate variability associated with the interdecadal Pacific oscillation. *J. Climate*, **26**, 7298–7310, https://doi.org/10.1175/JCLI-D-12-00548.1.

——, C. T. Y. Chung, J. M. Arblaster, M. M. Holland, and C. M. Bitz, 2018: Tropical decadal variability and the rate of Arctic sea ice decrease. *Geophys. Res. Lett.*, **45**, 11 326–11 333, https://doi.org/10.1029/2018GL079989.

Melia, N., K. Haines, E. Hawkins, and J. J. Day, 2017: Towards seasonal Arctic shipping route predictions. *Environ. Res. Lett.*, **12**, 084005, https://doi.org/10.1088/1748-9326/aa7a60.

Miles, M. W., D. V. Divine, T. Furevik, E. Jansen, M. Moros, and A. E. Ogilvie, 2014: A signal of persistent Atlantic multidecadal variability in Arctic sea ice. *Geophys. Res. Lett.*, **41**, 463–469, https://doi.org/10.1002/2013GL058084.

Milinski, S., N. Maher, and D. Olonscheck, 2020: How large does a large ensemble need to be? *Earth Syst. Dyn.*, **11**, 885–901, https://doi.org/10.5194/esd-11-885-2020.

Mioduszewski, J. R., S. Vavrus, M. Wang, M. Holland, and L. Landrum, 2019: Past and future interannual variability in Arctic sea ice in coupled climate models. *Cryosphere*, **13**, 113–124, https://doi.org/10.5194/tc-13-113-2019.

Murphy, L. N., J. M. Klavans, A. C. Clement, and M. A. Cane, 2021: Investigating the roles of external forcing and ocean circulation on the Atlantic multidecadal SST variability in a large ensemble climate model hierarchy. *J. Climate*, **34**, 4835–4849, https://doi.org/10.1175/JCLI-D-20-0167.1.

NASA Goddard Institute for Space Studies, 2018: NASA-GISS GISS-E2.1-G model output prepared for CMIP6 CMIP historical. Earth System Grid Federation, accessed 25 January 2023, https://doi.org/10.22033/ESGF/CMIP6.7127.

——, 2019a: NASA-GISS GISS-E2.2-G model output prepared for CMIP6 CMIP historical. Earth System Grid Federation, accessed 25 January 2023, https://doi.org/10.22033/ESGF/CMIP6.7129.

——, 2019b: NASA-GISS GISS-E2.1-H model output prepared for CMIP6 CMIP historical. Earth System Grid Federation, accessed 25 January 2023, https://doi.org/10.22033/ESGF/CMIP6.7128.

——, 2019c: NASA-GISS GISS-E2.2H model output prepared for CMIP6 CMIP historical. Earth System Grid Federation, accessed 25 January 2023, https://doi.org/10.22033/ESGF/CMIP6.15871.

Neubauer, D., and Coauthors, 2019: HAMMOZ-Consortium MPI-ESM1.2-HAM model output prepared for CMIP6 CMIP historical. Earth System Grid Federation, accessed 25 January 2023, https://doi.org/10.22033/ESGF/CMIP6.5016.

Notz, D., 2015: How well must climate models agree with observations? *Philos. Trans. Roy. Soc.*, **A373**, 20140164, https://doi.org/10.1098/rsta.2014.0164.

——, and J. Stroeve, 2016: Observed Arctic sea-ice loss directly follows anthropogenic CO_2 emission. *Science*, **354**, 747–750, https://doi.org/10.1126/science.aag2345.

Olonscheck, D., T. Mauritsen, and D. Notz, 2019: Arctic sea-ice variability is primarily driven by atmospheric temperature fluctuations. *Nat. Geosci.*, **12**, 430–434, https://doi.org/10.1038/s41561-019-0363-1.

Onarheim, I. H., T. Eldevik, L. H. Smedsrud, and J. C. Stroeve, 2018: Seasonal and regional manifestation of Arctic sea ice loss. *J. Climate*, **31**, 4917–4932, https://doi.org/10.1175/JCLI-D-17-0427.1.

O'Neill, B. C., and Coauthors, 2016: The Scenario Model Intercomparison Project (ScenarioMIP) for CMIP6. *Geosci. Model Dev.*, **9**, 3461–3482, https://doi.org/10.5194/gmd-9-3461-2016.

Petrick, S., K. Riemann-Campe, S. Hoog, C. Growitsch, H. Schwind, R. Gerdes, and K. Rehdanz, 2017: Climate change, future Arctic Sea ice, and the competitiveness of European Arctic offshore oil and gas production on world markets. *Ambio*, **46**, 410–422, https://doi.org/10.1007/s13280-017-0957-z.

Phillips, A., C. Deser, and J. Fasullo, 2014: Evaluating modes of variability in climate models. *Eos, Trans. Amer. Geophys. Union*, **95**, 453–455, https://doi.org/10.1002/2014EO490002.

Rayner, N. A., D. E. Parker, E. B. Horton, C. K. Folland, L. V. Alexander, D. P. Rowell, E. C. Kent, and A. Kaplan, 2003: Global analyses of sea surface temperature, sea ice, and night marine air temperature since the late nineteenth century. *J. Geophys. Res.*, **108**, 4407, https://doi.org/10.1029/2002JD002670.

Ridley, J., M. Menary, T. Kuhlbrodt, M. Andrews, and T. Andrews, 2019a: MOHC HadGEM3-GC31-LL model output prepared for CMIP6 CMIP historical. Earth System Grid Federation, accessed 25 January 2023, https://doi.org/10.22033/ESGF/CMIP6.6109.

——, ——, ——, ——, and ——, 2019b: MOHC HadGEM3-GC31-MM model output prepared for CMIP6 CMIP historical. Earth System Grid Federation, accessed 25 January 2023, https://doi.org/10.22033/ESGF/CMIP6.6112.

Roach, L. A., and E. Blanchard-Wrigglesworth, 2022: Observed winds crucial for September Arctic sea ice loss. *Geophys. Res. Lett.*, **49**, e2022GL097884, https://doi.org/10.1029/2022GL097884.

Rogers, J. C., 1981: The North Pacific Oscillation. *J. Climatol.*, **1**, 39–57, https://doi.org/10.1002/joc.3370010106.

Rong, X., 2019: CAMS CAMS_CSM1.0 model output prepared for CMIP6 CMIP historical. Earth System Grid Federation, accessed 25 January 2023, https://doi.org/10.22033/ESGF/CMIP6.9754.

Schupfner, M., and Coauthors, 2019: DKRZ MPI-ESM1.2-HR model output prepared for CMIP6 ScenarioMIP ssp245. Earth System Grid Federation, accessed 25 January 2023, https://doi.org/10.22033/ESGF/CMIP6.4398.

Screen, J. A., and C. Deser, 2019: Pacific Ocean variability influences the time of emergence of a seasonally ice-free Arctic Ocean. *Geophys. Res. Lett.*, **46**, 2222–2231, https://doi.org/10.1029/2018GL081393.

Seferian, R., 2018: CNRM-CERFACS CNRM-ESM2-1 model output prepared for CMIP6 CMIP historical. Earth System Grid Federation, accessed 25 January 2023, https://doi.org/10.22033/ESGF/CMIP6.4068.

Seland, Ø., and Coauthors, 2019: NCC NorESM2-LM model output prepared for CMIP6 CMIP historical. Earth System Grid Federation, accessed 25 January 2023, https://doi.org/10.22033/ESGF/CMIP6.8036.

Serreze, M. C., M. M. Holland, and J. Stroeve, 2007: Perspectives on the Arctic's shrinking sea-ice cover. *Science*, **315**, 1533–1536, https://doi.org/10.1126/science.1139426.

Sigmond, M., J. C. Fyfe, and N. C. Swart, 2018: Ice-free Arctic projections under the Paris Agreement. *Nat. Climate Change*, **8**, 404–408, https://doi.org/10.1038/s41558-018-0124-y.

Simon, A., G. Gastineau, C. Frankignoul, V. Lapin, and P. Ortega, 2022: Pacific decadal oscillation modulates the Arctic sea-ice loss influence on the midlatitude atmospheric circulation in winter. *Wea. Climate Dyn.*, **3**, 845–861, https://doi.org/10.5194/wcd-3-845-2022.

Song, Z., F. Qiao, Y. Bao, Q. Shu, Y. Song, and X. Yang, 2019: FIO-QLNM FIO-ESM2.0 model output prepared for CMIP6 CMIP historical. Earth System Grid Federation, accessed 25 January 2023, https://doi.org/10.22033/ESGF/CMIP6.9199.

Stroeve, J., M. M. Holland, W. Meier, T. Scambos, and M. Serreze, 2007: Arctic sea ice decline: Faster than forecast. *Geophys. Res. Lett.*, **34**, L09501, https://doi.org/10.1029/2007GL029703.

Swart, N. C., J. C. Fyfe, E. Hawkins, J. E. Kay, and A. Jahn, 2015: Influence of internal variability on arctic sea-ice trends. *Nat. Climate Change*, **5**, 86–89, https://doi.org/10.1038/nclimate2483.

——, and Coauthors, 2019a: CCCma CanESM5-CanOE model output prepared for CMIP6 CMIP historical. Earth System Grid Federation, accessed 25 January 2023, https://doi.org/10.22033/ESGF/CMIP6.10260.

——, and Coauthors, 2019b: CCCma CanESM5 model output prepared for CMIP6 CMIP historical. Earth System Grid Federation, accessed 25 January 2023, https://doi.org/10.22033/ESGF/CMIP6.3610.

Tang, Y., S. Rumbold, R. Ellis, D. Kelley, J. Mulcahy, A. Sellar, J. Walton, and C. Jones, 2019: MOHC UKESM1.0-LL model output prepared for CMIP6 CMIP historical. Earth System Grid Federation, accessed 25 January 2023, https://doi.org/10.22033/ESGF/CMIP6.6113.

Tatebe, H., and M. Watanabe, 2018: MIROC MIROC6 model output prepared for CMIP6 CMIP historical. Earth System Grid Federation, accessed 25 January 2023, https://doi.org/10.22033/ESGF/CMIP6.5603.

Tietsche, S., and Coauthors, 2014: Seasonal to interannual Arctic sea ice predictability in current global climate models. *Geophys. Res. Lett.*, **41**, 1035–1043, https://doi.org/10.1002/2013GL058755.

Topál, D., Q. Ding, J. Mitchell, I. Baxter, M. Herein, T. Haszpra, R. Luo, and Q. Li, 2020: An internal atmospheric process determining summertime Arctic sea ice melting in the next three decades: Lessons learned from five large ensembles and multiple CMIP5 climate simulations. *J. Climate*, **33**, 7431–7454, https://doi.org/10.1175/JCLI-D-19-0803.1.

Trenberth, K. E., 1997: The definition of El Niño. *Bull. Amer. Meteor. Soc.*, **78**, 2771–2778, https://doi.org/10.1175/1520-0477(1997)078<2771:TDOENO>2.0.CO;2.

——, and D. J. Shea, 2006: Atlantic hurricanes and natural variability in 2005. *Geophys. Res. Lett.*, **33**, L12704, https://doi.org/10.1029/2006GL026894.

Ukita, J., M. Honda, H. Nakamura, Y. Tachibana, D. J. Cavalieri, C. L. Parkinson, H. Koide, and K. Yamamoto, 2007: Northern Hemisphere sea ice variability: Lag structure and its implications. *Tellus*, **59A**, 261–272, https://doi.org/10.1111/j.1600-0870.2006.00223.x.

VanAchter, G., L. Ponsoni, F. Massonnet, T. Fichefet, and V. Legat, 2020: Brief communication: Arctic sea ice thickness internal variability and its changes under historical and anthropogenic forcing. *Cryosphere*, **14**, 3479–3486, https://doi.org/10.5194/tc-14-3479-2020.

Vance, T. R., A. S. Kiem, L. M. Jong, J. L. Roberts, C. T. Plummer, A. D. Moy, M. A. J. Curran, and T. D. van Ommen, 2022: Pacific decadal variability over the last 2000 years and implications for climatic risk. *Commun. Earth Environ.*, **3**, 33, https://doi.org/10.1038/s43247-022-00359-z.

Voldoire, A., 2018: CMIP6 simulations of the CNRM-CERFACS based on CNRM-CM6-1 model for CMIP experiment historical. Earth System Grid Federation, accessed 25 January 2023, https://doi.org/10.22033/ESGF/CMIP6.4066.

Volodin, E., and Coauthors, 2019: INM INM-CM5-0 model output prepared for CMIP6 CMIP historical. Earth System Grid Federation, accessed 25 January 2023, https://doi.org/10.22033/ESGF/CMIP6.5070.

Wang, M., and J. E. Overland, 2012: A sea ice free summer Arctic within 30 years: An update from CMIP5 models. *Geophys. Res. Lett.*, **39**, L18501, https://doi.org/10.1029/2012GL052868.

Wang, Q., S. Danilov, L. Mu, D. Sidorenko, and C. Wekerle, 2021: Lasting impact of winds on Arctic sea ice through the ocean's memory. *Cryosphere*, **15**, 4703–4725, https://doi.org/10.5194/tc-15-4703-2021.

Watanabe, S., and Coauthors, 2021: MIROC MIROC-ES2H model output prepared for CMIP6 CMIP historical. Earth System Grid Federation, accessed 25 January 2023, https://doi.org/10.22033/ESGF/CMIP6.5601.

Weijer, W., W. Cheng, O. A. Garuba, A. Hu, and B. T. Nadiga, 2020: CMIP6 models predict significant 21st century decline of the Atlantic meridional overturning circulation. *Geophys. Res. Lett.*, **47**, e2019GL086075, https://doi.org/10.1029/2019GL086075.

Wieners, K.-H., and Coauthors, 2019: MPI-M MPIESM1.2-LR model output prepared for CMIP6 historical. Earth System Grid Federation, accessed 25 January 2023, https://doi.org/10.22033/ESGF/CMIP6.6595.

Wu, T., and Coauthors, 2018: BCC BCC-CSM2MR model output prepared for CMIP6 CMIP historical. Earth System Grid Federation, accessed 25 January 2023, https://doi.org/10.22033/ESGF/CMIP6.2948.

Wyburn-Powell, C., A. Jahn, and M. R. England, 2022: Modeled interannual variability of Arctic sea ice cover is within observational uncertainty. *J. Climate*, **35**, 6827–6842, https://doi.org/10.1175/JCLI-D-21-0958.1.

Yeager, S. G., A. R. Karspeck, and G. Danabasoglu, 2015: Predicted slowdown in the rate of Atlantic sea ice loss. *Geophys. Res. Lett.*, **42**, 10 704–10 713, https://doi.org/10.1002/2015GL065364.

Yuan, X., M. R. Kaplan, and M. A. Cane, 2018: The interconnected global climate system—A review of tropical–polar teleconnections. *J. Climate*, **31**, 5765–5792, https://doi.org/10.1175/JCLI-D-16-0637.1.

Yukimoto, S., and Coauthors, 2019: MRI MRI-ESM2.0 model output prepared for CMIP6 CMIP historical. Earth System Grid Federation, accessed 25 January 2023, https://doi.org/10.22033/ESGF/CMIP6.6842.

Zebiak, S. E., 1993: Air–sea interaction in the equatorial Atlantic region. *J. Climate*, **6**, 1567–1586, https://doi.org/10.1175/1520-0442(1993)006<1567:AIITEA>2.0.CO;2.

Zhang, R., 2015: Mechanisms for low-frequency variability of summer Arctic sea ice extent. *Proc. Natl. Acad. Sci. USA*, **112**, 4570–4575, https://doi.org/10.1073/pnas.1422296112.

Zhang, J., and Coauthors, 2018: BCC BCC-ESM1 model output prepared for CMIP6 CMIP historical. Earth System Grid Federation, accessed 25 January 2023, https://doi.org/10.22033/ESGF/CMIP6.2949.

Zhang, M., W. Perrie, and Z. Long, 2019: Springtime North Pacific Oscillation and summer sea ice in the Beaufort sea. *Climate Dyn.*, **53**, 671–686, https://doi.org/10.1007/s00382-019-04627-1.

Zhang, S., T. Y. Gan, and A. B. Bush, 2020: Variability of Arctic sea ice based on quantile regression and the teleconnection with large-scale climate patterns. *J. Climate*, **33**, 4009–4025, https://doi.org/10.1175/JCLI-D-19-0375.1.

Ziehn, T., and Coauthors, 2019: CSIRO ACCESS-ESM1.5 model output prepared for CMIP6 CMIP historical. Earth System Grid Federation, accessed 25 January 2023, https://doi.org/10.22033/ESGF/CMIP6.4272.